Pulsars: excellent systems for testing particle acceleration theories

広谷 幸一

Kouichi HIROTANI

高等理論天文物理学研究中心/清華大

TIARA/ASIAA-NTHU, Taiwan

IPMU

March 16, 2009

Crab nebula: Composite image of X-ray [blue] and optical [red]

§1 Introduction: Why γ-ray?

Observing the Universe in γ-rays allows us to examine the matter-radiation interactions under extreme conditions (high T, high density, strong $\boldsymbol{B}$).

e.g., ●inverse-Compton scatterings in extra-galactic jets,
●curvature radiation from young neutron stars in Our Galaxy.

γ-ray sky (>100 MeV)

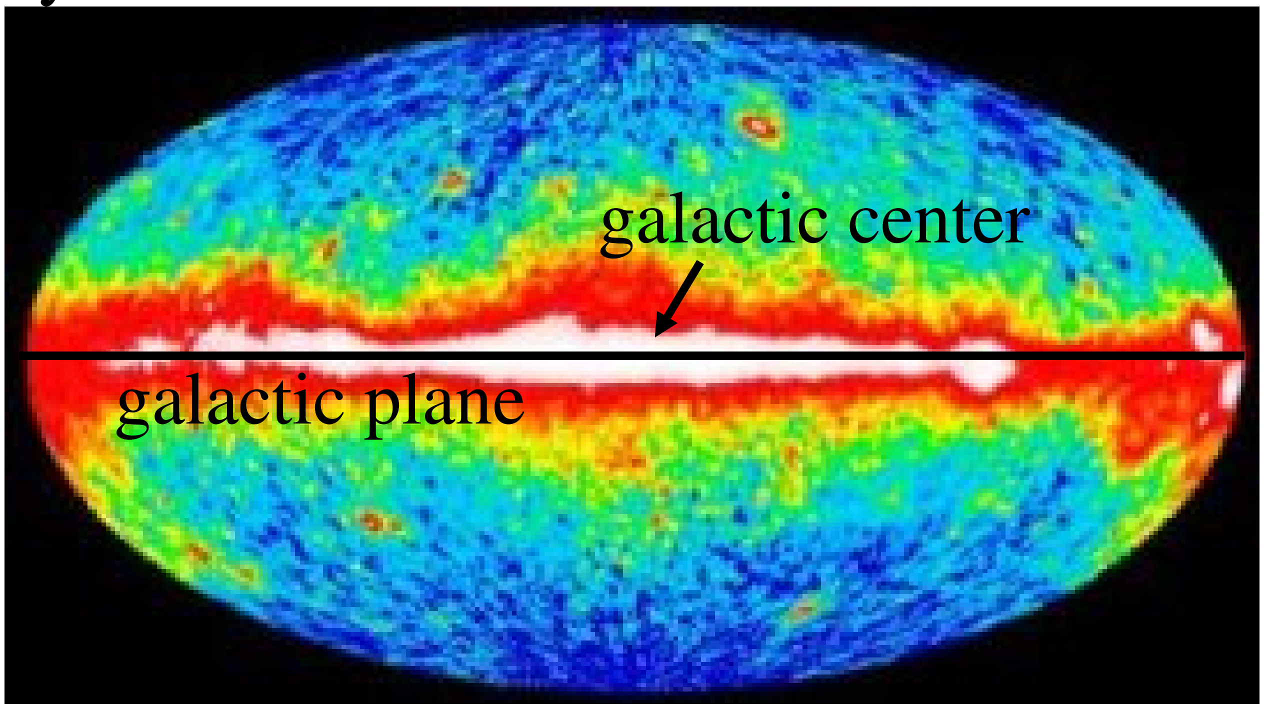

§1 Introduction: Why γ-ray?

Observing the Universe in γ-rays allows us to examine the matter-radiation interactions under extreme conditions (high T, high density, strong $\boldsymbol{B}$).

e.g., ●inverse-Compton scatterings in extra-galactic jets,
●curvature radiation from young neutron stars in Our Galaxy.

In addition, the Universe is largely transparent to γ-rays.

Small interaction cross sections $\longrightarrow$ direct view into high-energy acceleration processes

Since γ-rays cannot transmit the atmosphere, we have to launch balloons or satellites to observe in γ-ray energies.

§1 Introduction: Two γ-ray telescopes

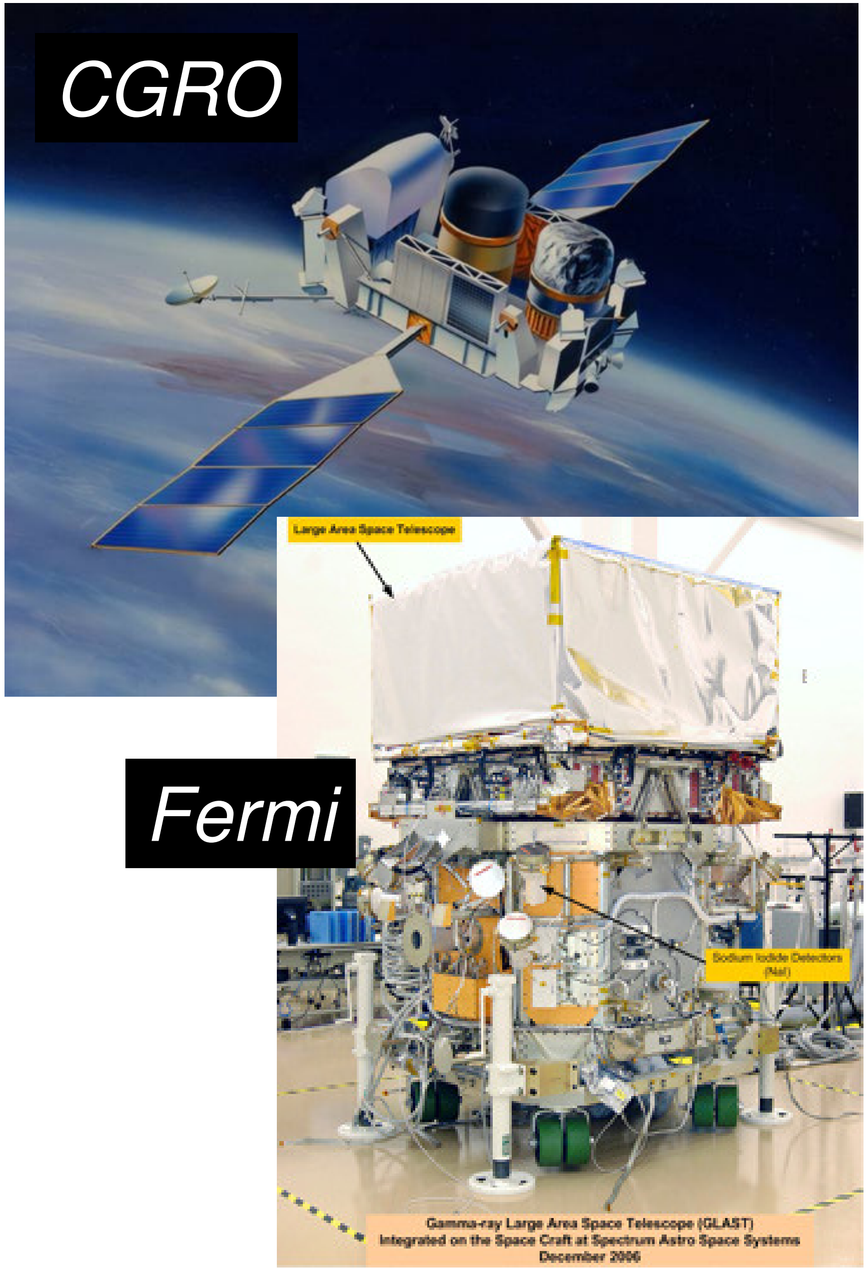

The *Energetic Gamma-Ray Experiment Telescope* (*EGRET*) aboard *Compton Gamma-Ray Observatory* (*CGRO*) has detected 271 steady (not transient) point sources above 30 MeV (1991-1996).

The *Large Area Telescope* (*LAT*) aboard *Fermi Gamma-Ray Space Telescope* is detecting more point sources (2008, Abdo+, Science).

§1 Introduction: The γ-ray sky

Among those (more than 270) point sources, **pulsars** are the most luminous objects in the γ-ray sky.

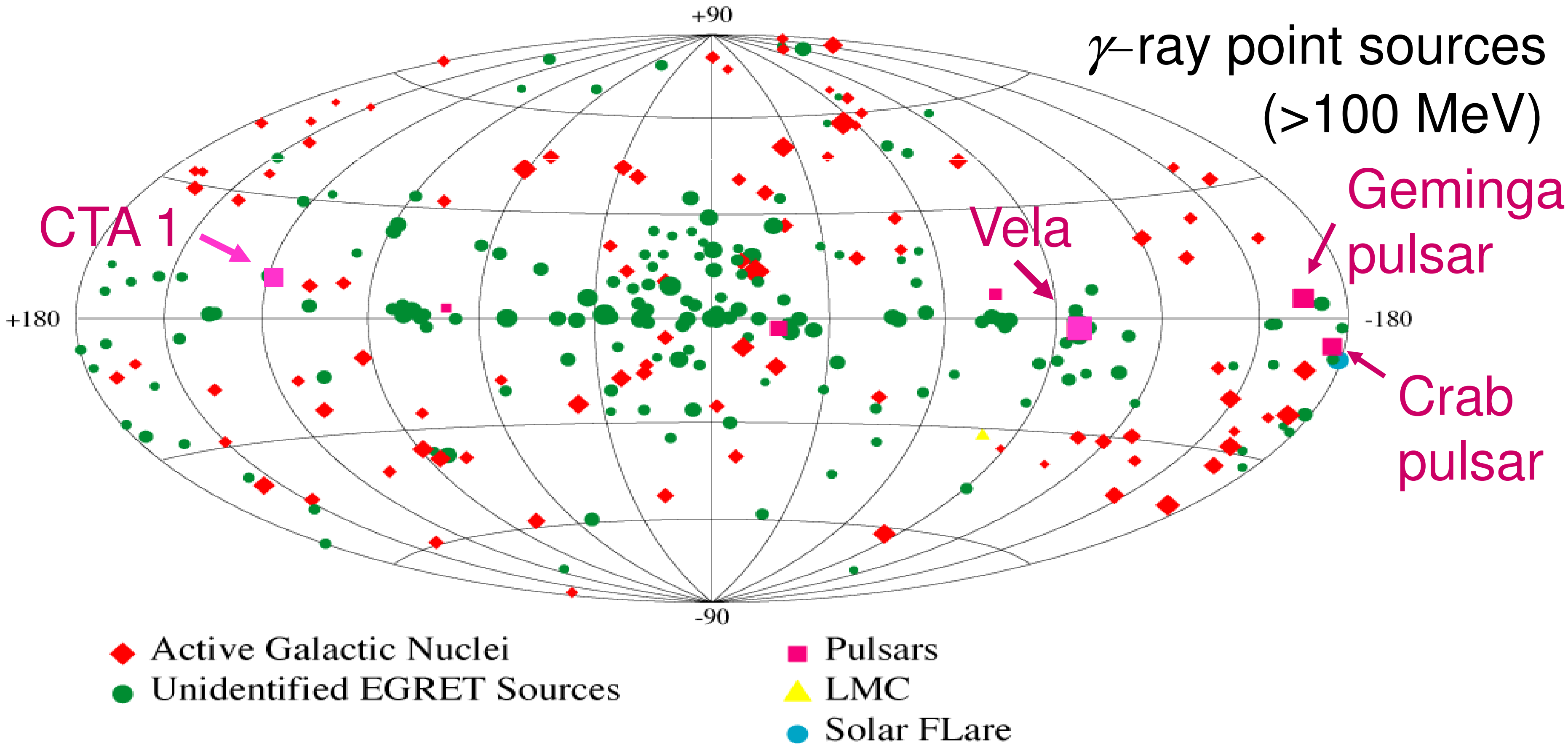

§1 Introduction: The γ-ray sky

Pulsars:

rapidly rotating, highly magnetized neutrons stars (NS)

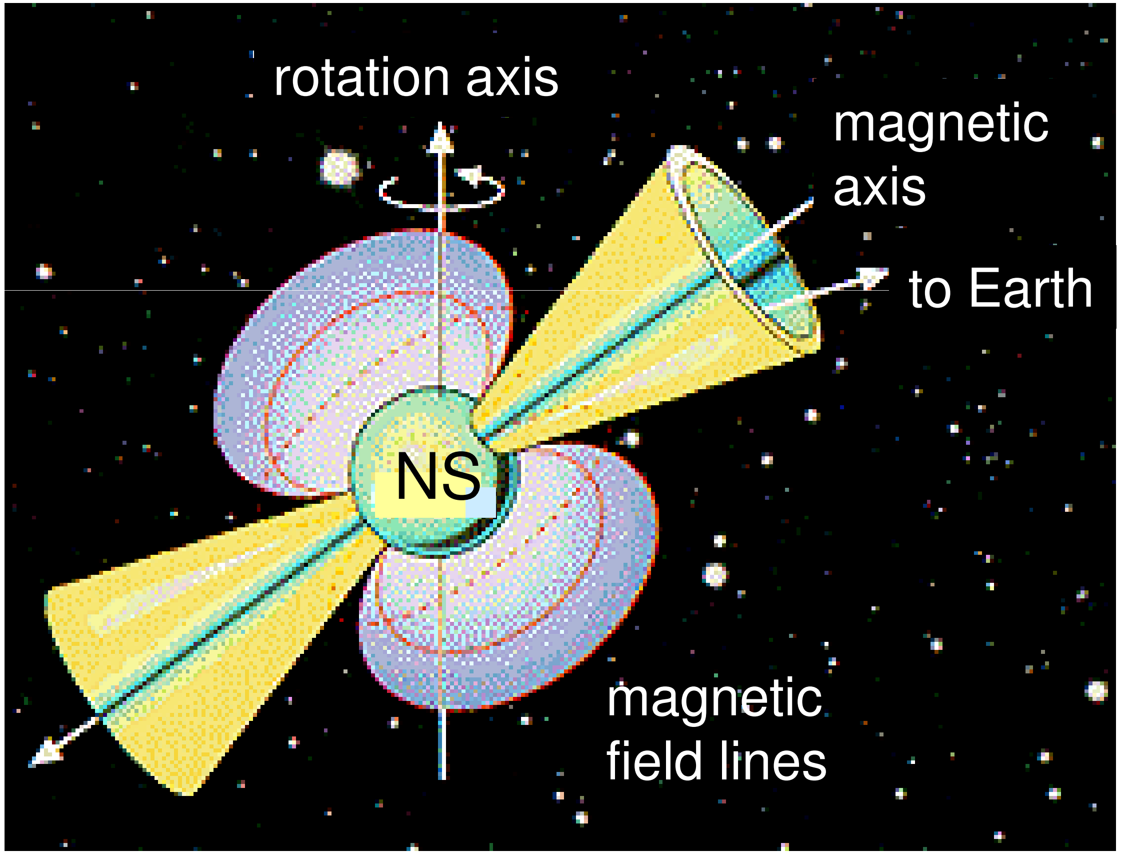

The ***B*** and rotation axes are misaligned.

The beam of light sweep around as NS rotates (e.g., lighthouse).

Pulsars turn on and off as the beam sweeps our line of sight.

§1 γ-ray Observations of Pulsars

9 pulsars confirmed above 100 MeV.

J1028-5819: (ApJL in press)
no pulse profile available

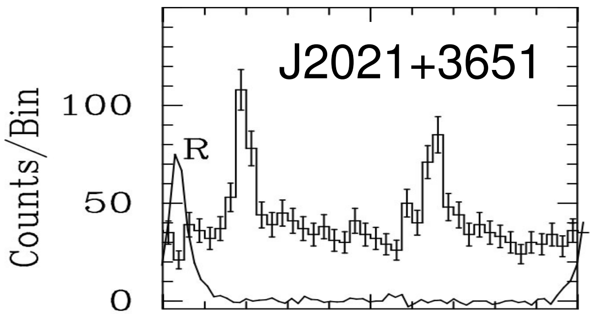

AGILE (Halpern+08)

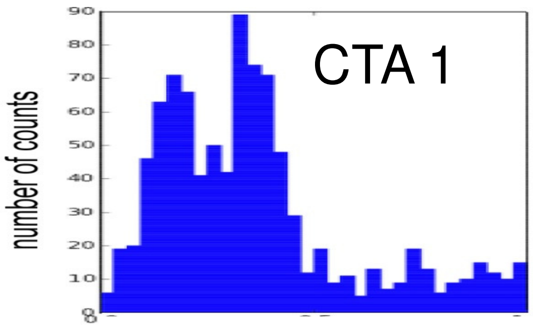

LAT (Abdo+ 08)

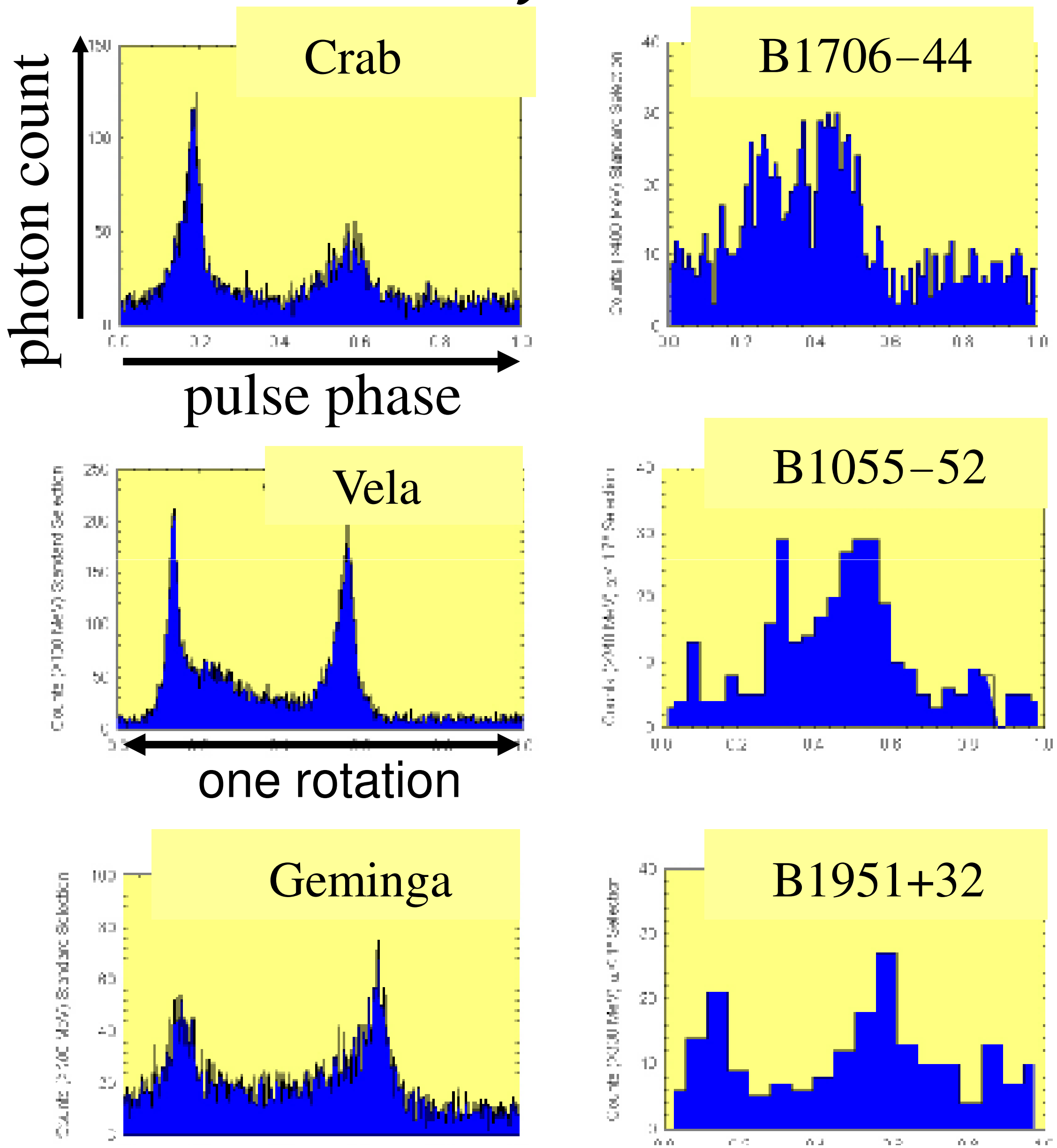

EGRET (Thompson 01, Kanbach 02)

§1 γ-ray Observations of Pulsars

9 pulsars confirmed above 100 MeV.

Doube-peak pulse profile is common.

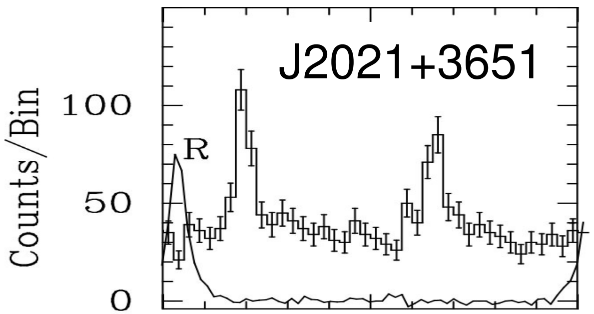

AGILE (Halpern+08)

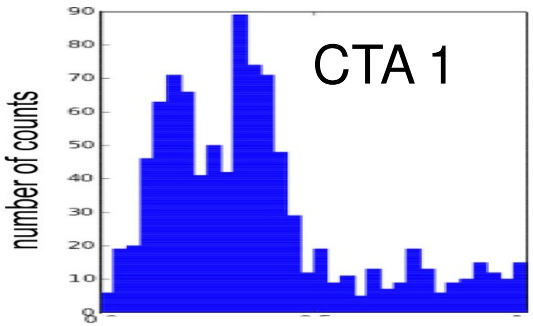

LAT (Abdo+ 08)

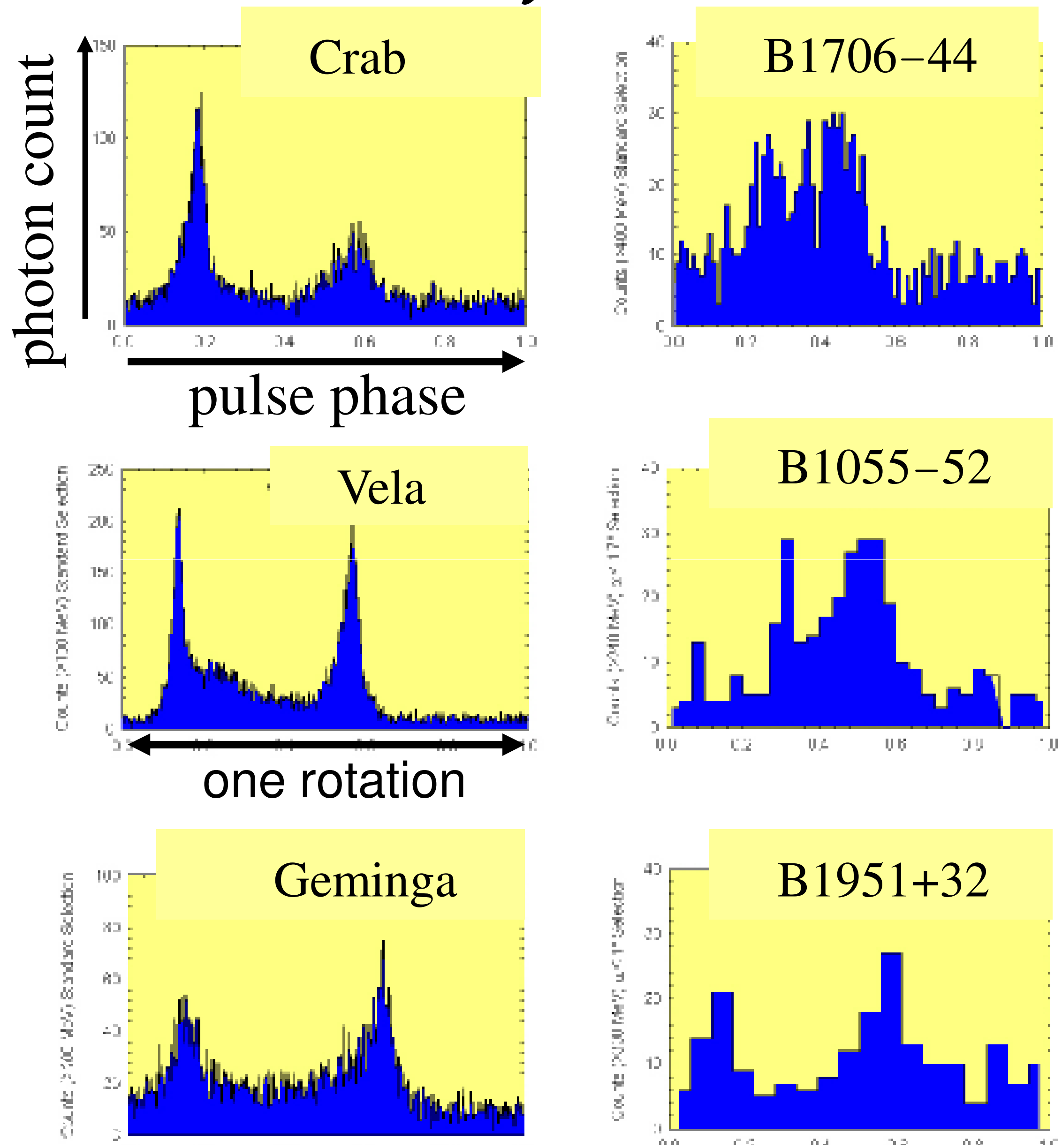

EGRET (Thompson 01, Kanbach 02)

Broad-band spectra (pulsed)

- Power peaks in γ-rays
- No pulsed emission above 30 GeV
- High-energy turnover
- Spectrum gets harder as the NS ages. E.g., the **Crab** pulsar shows very soft γ-ray spectrum.
- B1951+32 shows the hardest spectrum.

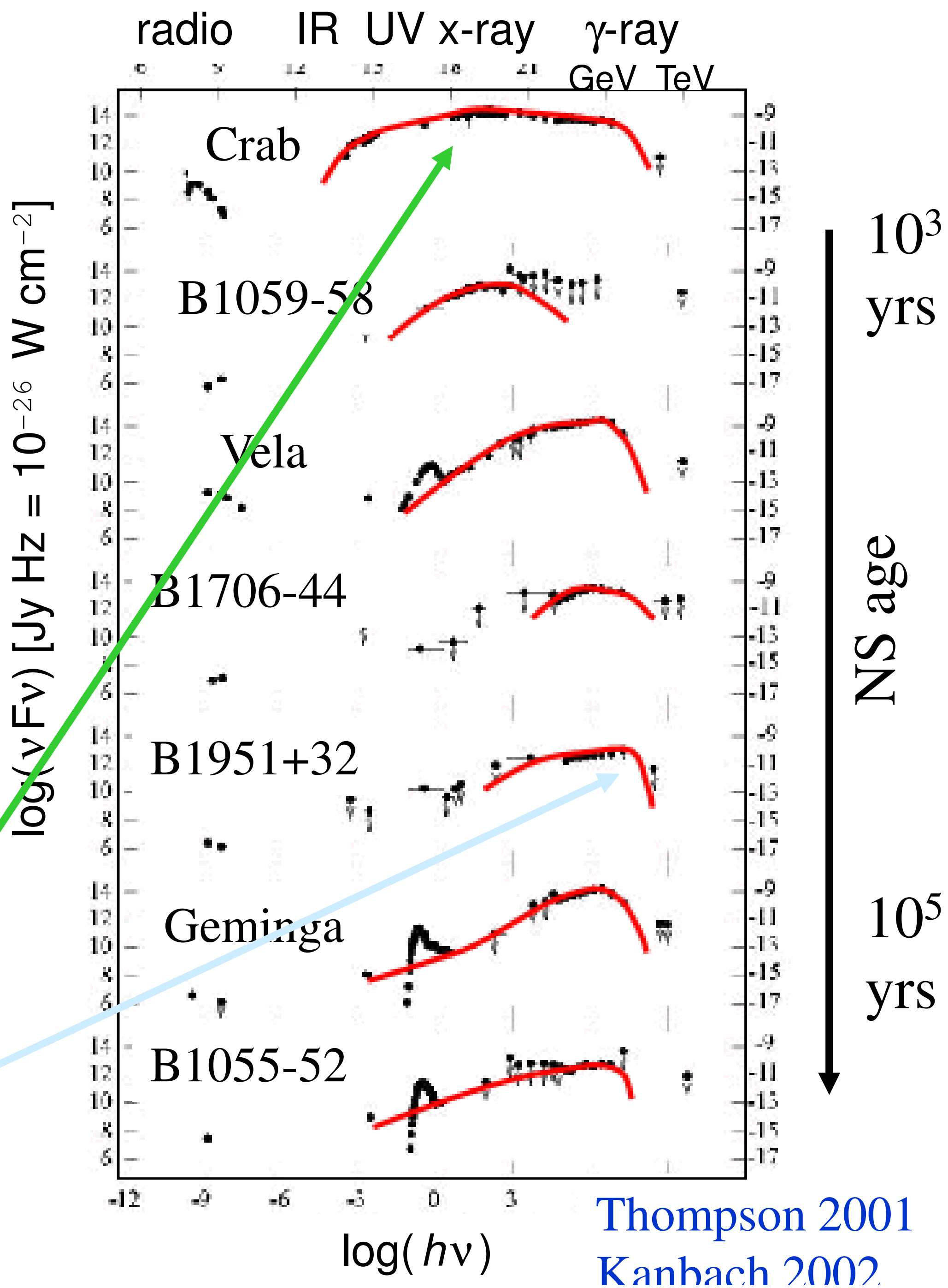

Thompson 2001
Kanbach 2002

Broad-band spectra (pulsed)

●High-energy (>100MeV) photons are emitted via **curvature** process by ultra-relativistic (~10 TeV) $e^{\pm}$'s accelerated in pulsar magnetosphere.

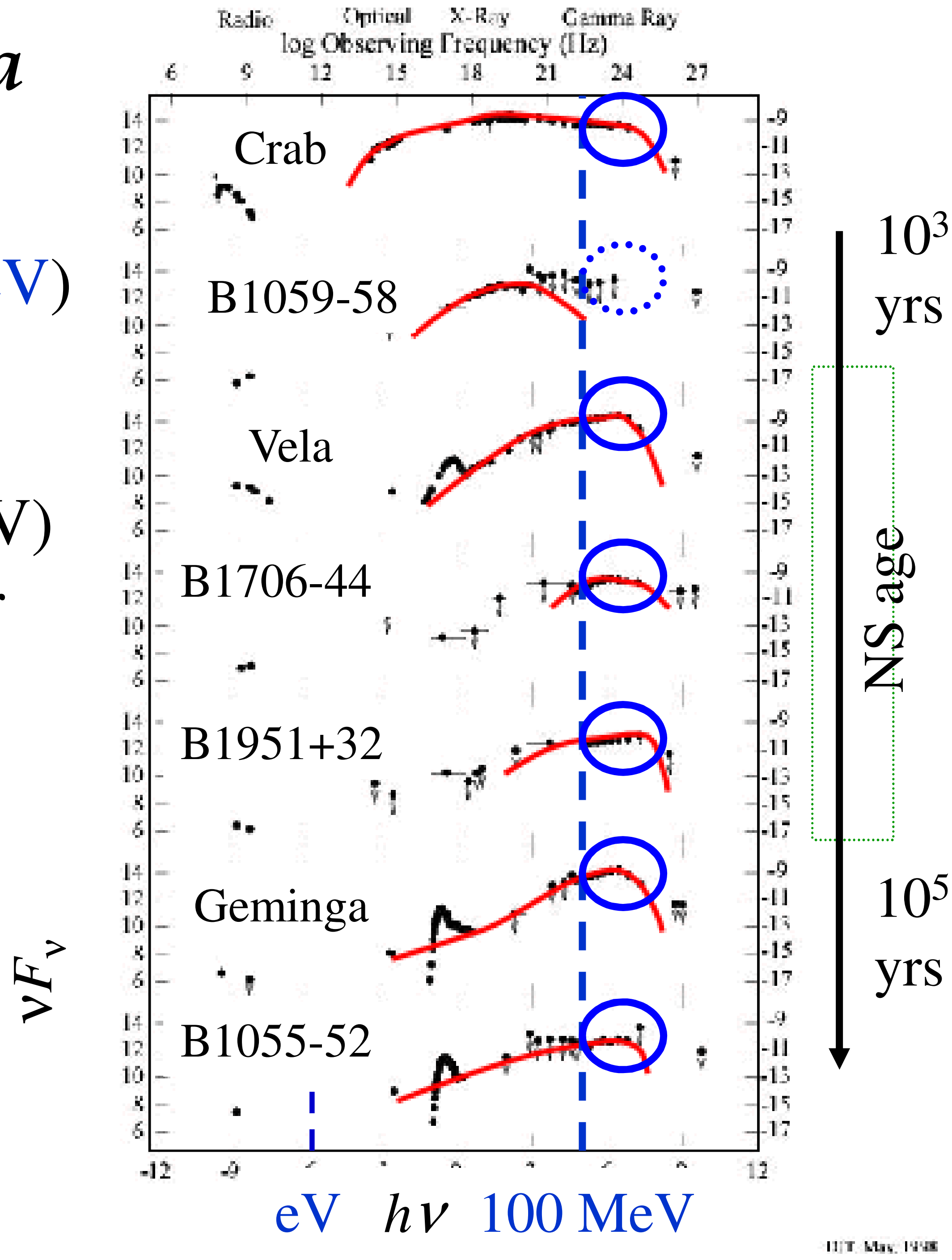

Broad-band spectra (pulsed)

- High-energy (>100MeV) photons are emitted via **curvature** process by ultra-relativistic (~10 TeV) $e^{\pm}$'s accelerated in pulsar magnetosphere.

- Some of such **primary γ-rays** are absorbed in the NS magnetosphere and reprocessed in lower energies via **synchrotron** process.

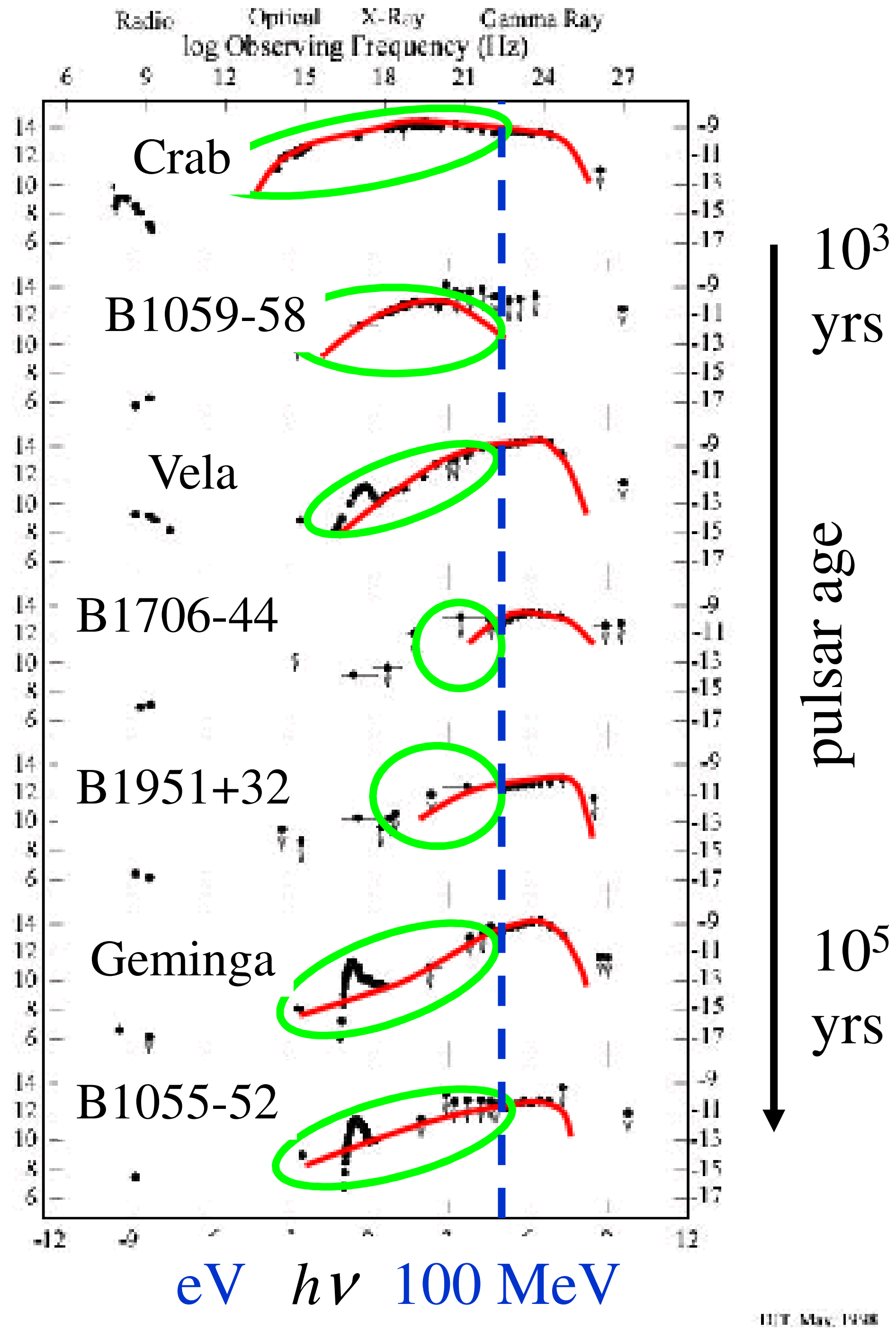

§1 γ-ray Observations of Pulsars

Among ~1800 known rotation-powered pulsars, only nine have been firmly detected above 100 MeV.

Nevertheless, in spite of their paucity, γ-ray observations are a valuable tool for studying particle acceleration in relativistic energies.

Structure of this talk

§1 Introduction

§2 Basic mechanisms of particle acceleration

§3 Traditional Emission Models

§4 New Gap Theory: Analytical Approach

Hirotani (2008, ApJ 688, L25)

§5 New Gap Theory: Numerical Approach

Hirotani (2008, submitted to Open Astronomy)

§2 Basic Emission Mechanism

Pulsar emissions result from electro-dynamical extraction of NS rotational energy.

On the spinning NS surface,
EMF is exerted (fig).

This EMF induces the global current, which extracts the rotational energy as Poynting flux.

In the case of pulsars, EMF is available only within the so-called 'open zone'.

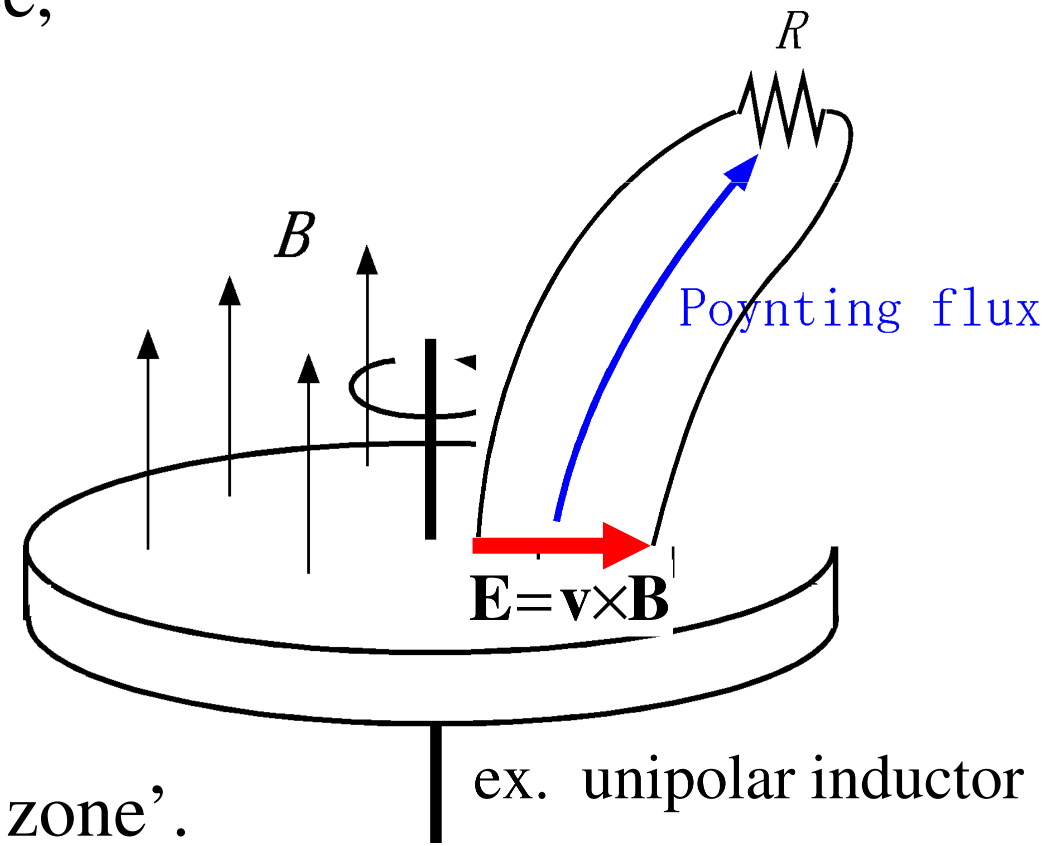

ex. unipolar inductor

§2 Basic Emission Mechanism

A rotating NS magnetosphere can be divided into open and closed zones.

Last-open field lines form the boundary of them.

In the open zone, $e^{\pm}$'s escape through the light cylinder as a pulsar wind.

In the closed zone, on the other hand, an $E_{\parallel}$ would be very quickly screened by the dense plasmas.

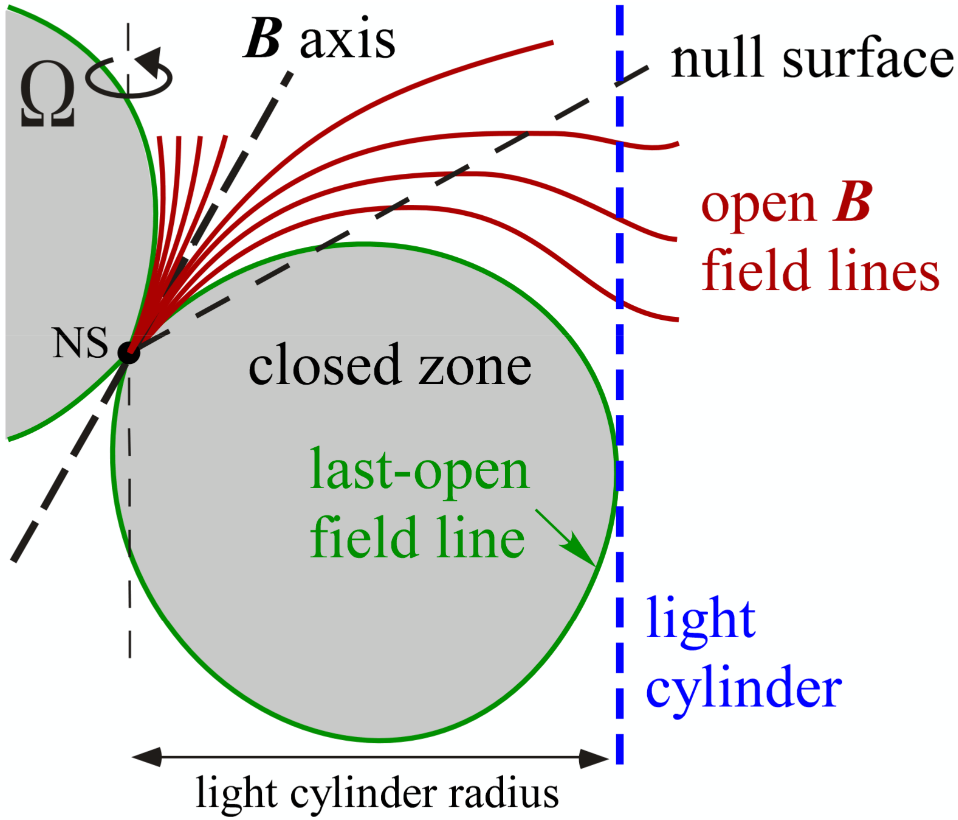

$$\varpi_{LC} = 3\times10^{8}(\Omega/10^{2}\,\mathrm{rad\,s^{-1}})\ \mathrm{cm}$$

§2 Basic Emission Mechanism

A rotating NS magnetosphere can be divided into open and closed zones.

Last-open field lines form the boundary of them.

In the open zone, $e^{\pm}$'s escape through the light cylinder as a pulsar wind.

In the closed zone, on the other hand, an $E_{||}$ would be very quickly screened by the dense plasmas.

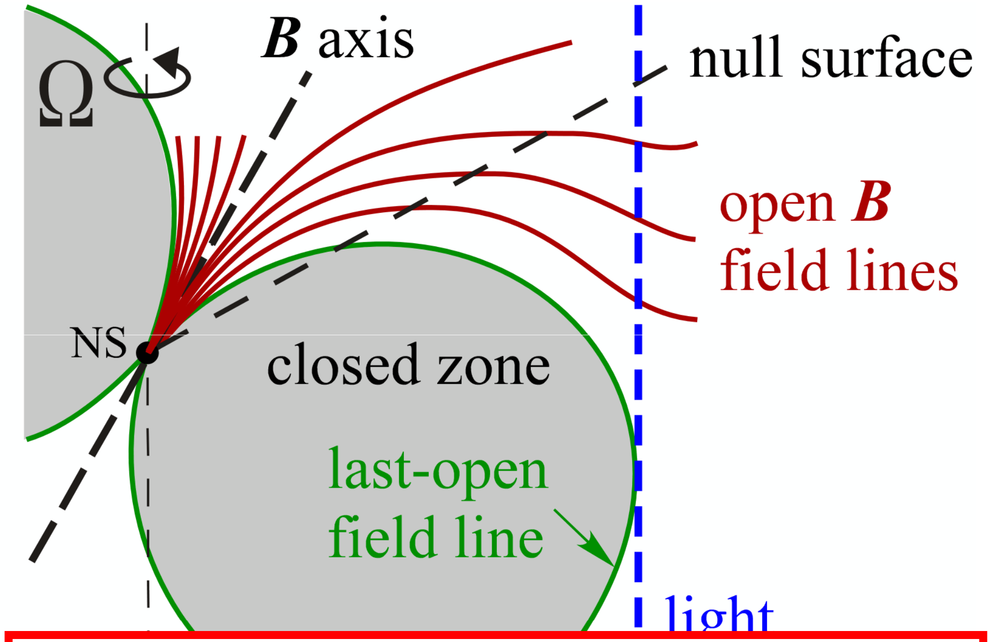

Thus, in all pulsar emission models, particle acceleration takes place only within the open zone.

§2 *Basic Emission Mechanism*

For typical high-energy pulsars, open zone occupies only a few degrees from ***B*** axis on the PC surface.

Available voltage in the open zone:

$$\mathrm{EMF} \sim \frac{\Omega^2 B_* r_*^3}{c^2} \sim 10^{15.5}\ \mathrm{V}$$

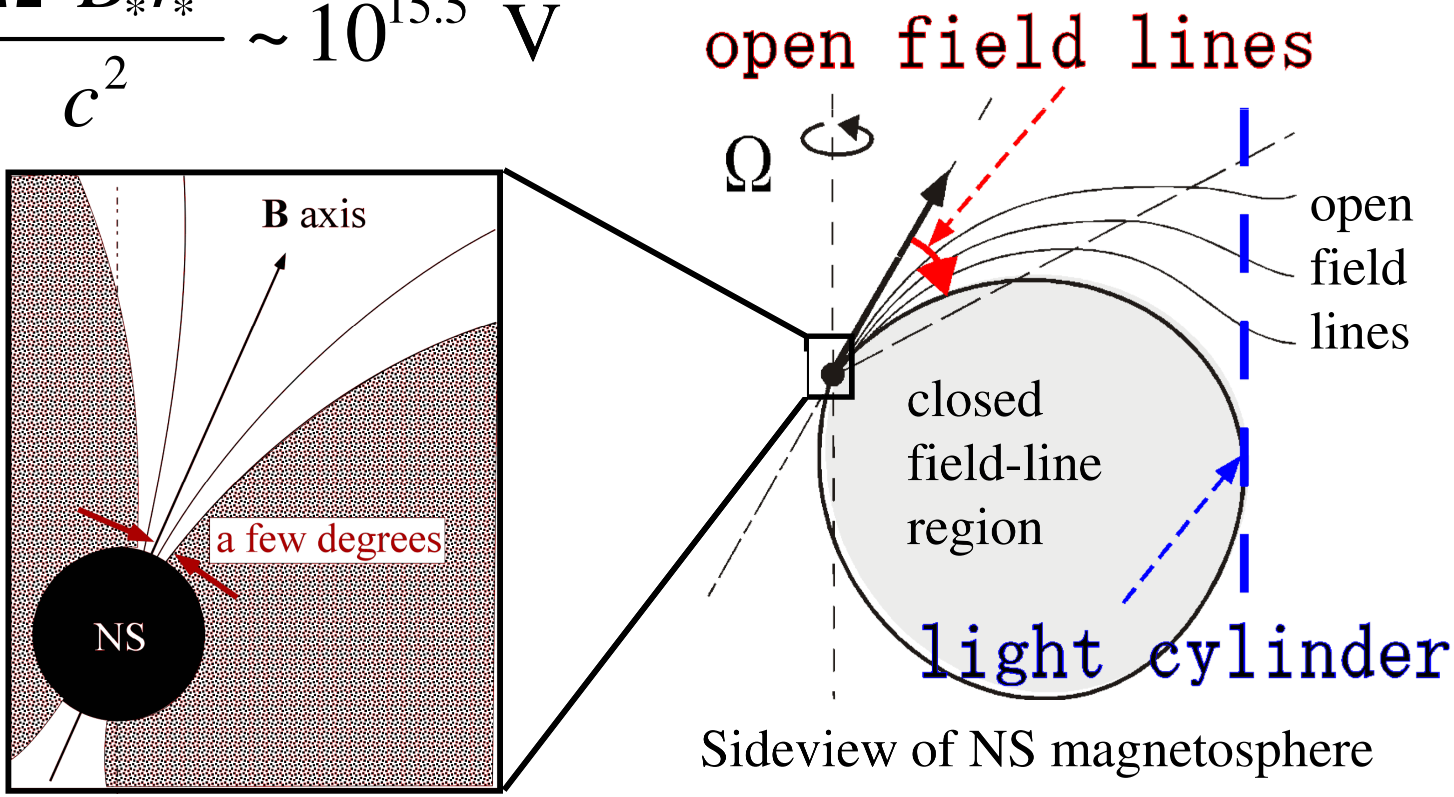

Sideview of NS magnetosphere

§2 Basic Emission Mechanism

For typical high-energy pulsars, open zone occupies only a few degrees from ***B*** axis on the PC surface.

Available voltage:

$$\mathrm{EMF} \sim \frac{\Omega^2 B_* r_*^3}{c^2} \sim 10^{15.5}\ \mathrm{V}$$

A fraction (0.1~20%) of this EMF is used for pulsed γ-ray emission within the light cylinder.

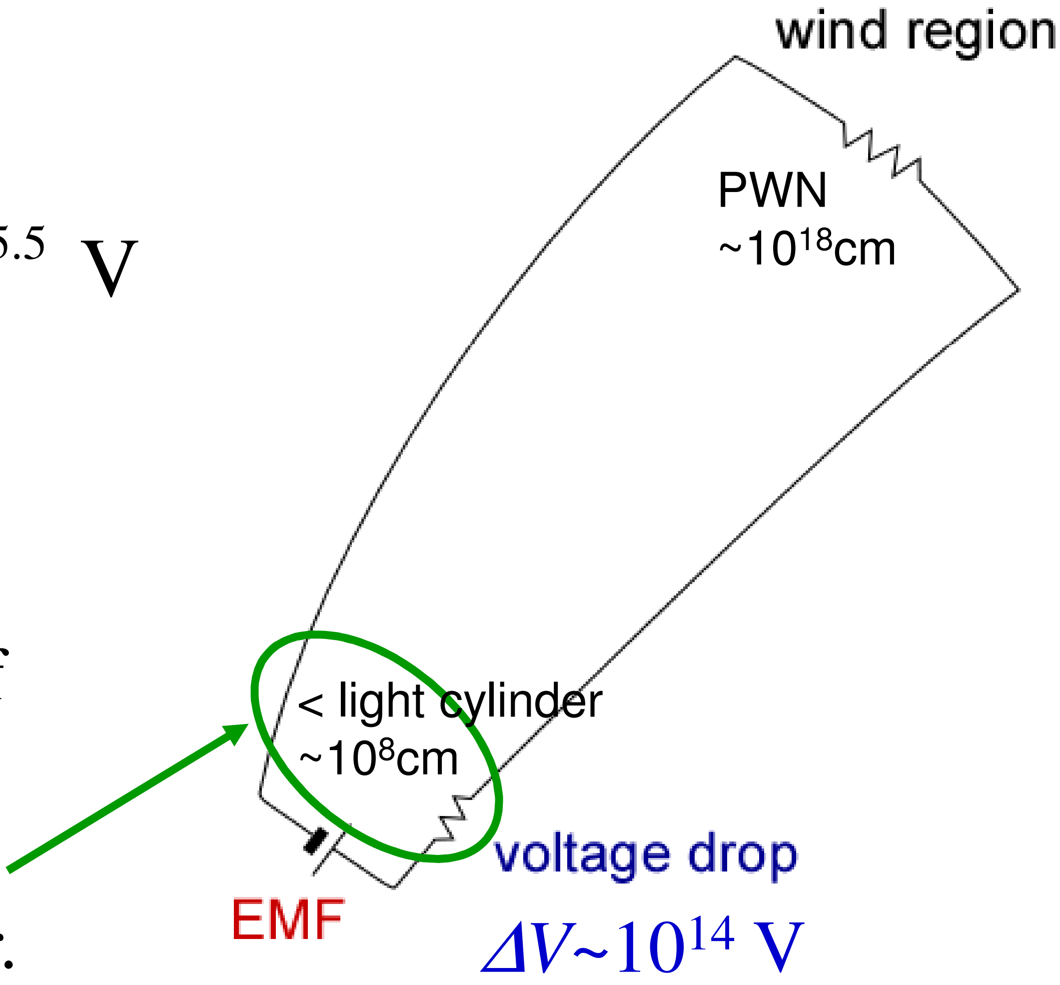

§2 Basic Emission Mechanism

Available voltage:

$$\mathrm{EMF} \sim \frac{\Omega^2 B_* r_*^3}{c^2} \sim 10^{15.5}\ \mathrm{V}$$

Today, I will concentrate how this small voltage drop ($<\varpi_{\mathrm{LC}}$) is converted into pulsed high-energy emission.

A fraction (0.1~20%) of this EMF is used for pulsed γ-ray emission within the light cylinder.

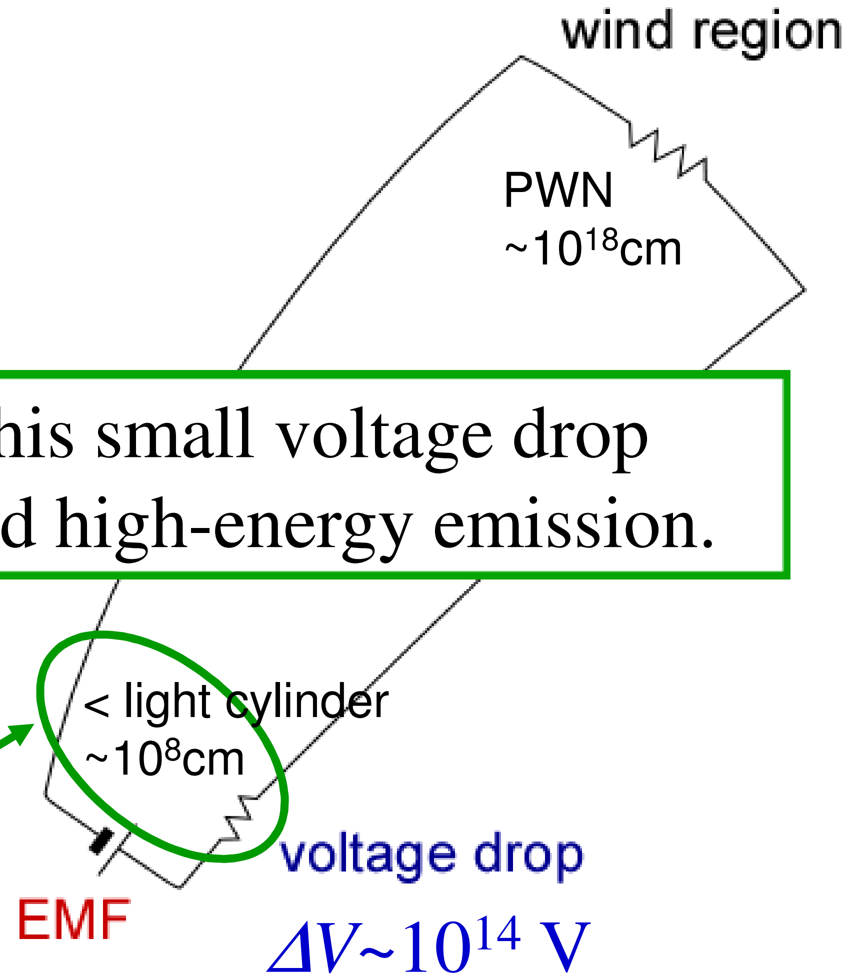

§2 Basic Emission Mechanism

In a rotating NS magnetosphere, the Goldreich-Julian charge density is induced for a static observer.

Decoupling $\mathbf{E}$ into $\mathbf{E}_\perp$ and $\mathbf{E}_{||}$, we obtain the Maxwell eq.,

$$\nabla \cdot \left(\mathbf{E}_\perp + \mathbf{E}_{||}\right) = 4\pi\rho,$$

where $\rho \equiv e(n_+ - n_-)$, and $\mathbf{E}_\perp \equiv -c^{-1}(\mathbf{\Omega}\times\mathbf{r})\times\mathbf{B}$.

Concentrating on the acceleration term, $\nabla \cdot \mathbf{E}_{||}$, one obtains

$$\nabla \cdot \mathbf{E}_{||} = 4\pi(\rho - \rho_{\mathrm{GJ}}),$$

where

$$\rho_{\mathrm{GJ}} \equiv \frac{1}{4\pi}\nabla \cdot \mathbf{E}_\perp = -\frac{\mathbf{\Omega}\cdot\mathbf{B}}{2\pi c}.$$

That is, ρ_{GJ} is uniquely determined by B-field geometry.

§2 Basic Emission Mechanism

In a rotating NS magnetosphere, the Goldreich-Julian charge density is induced for a static observer.

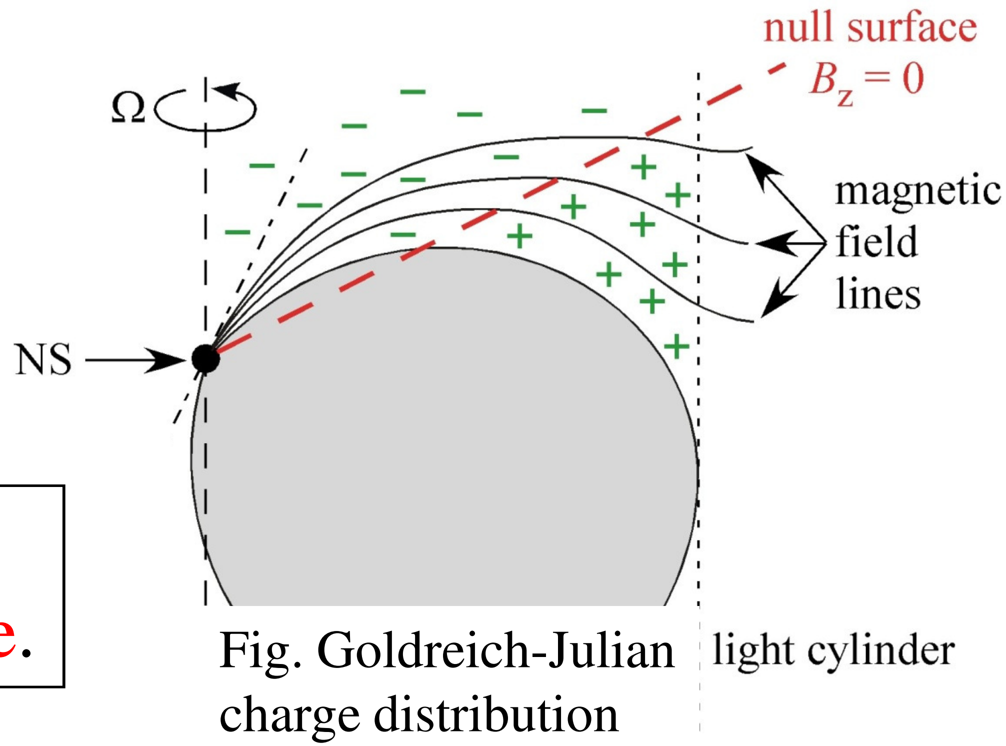

Fig. Goldreich-Julian charge distribution (side view)

Note that $\rho_{\rm GJ}$ changes sign at the null surface.

$$\rho_{\rm GJ} \equiv \frac{1}{4\pi} \nabla \cdot \mathbf{E}_\perp = -\frac{\mathbf{\Omega} \cdot \mathbf{B}}{2\pi c}.$$

§3 Traditional Emission Models

Next question:

Where is the particle accelerator, in which $\boldsymbol{E}_{||}$ arises?

§3 Traditional Emission Models

Attempts to model high-energy emissions concentrate on three scenarios:

- **inner gap (polar cap)**
  (Daugherty & Harding 1996 ApJ 458, 278)
- **slot gap**
  (Arons 1983, ApJ 302, 301; Muslimov & Harding 2004, ApJ 606, 1143)
- **outer gap**
  (Cheng, Ho, Ruderman 1986, ApJ 300, 500)

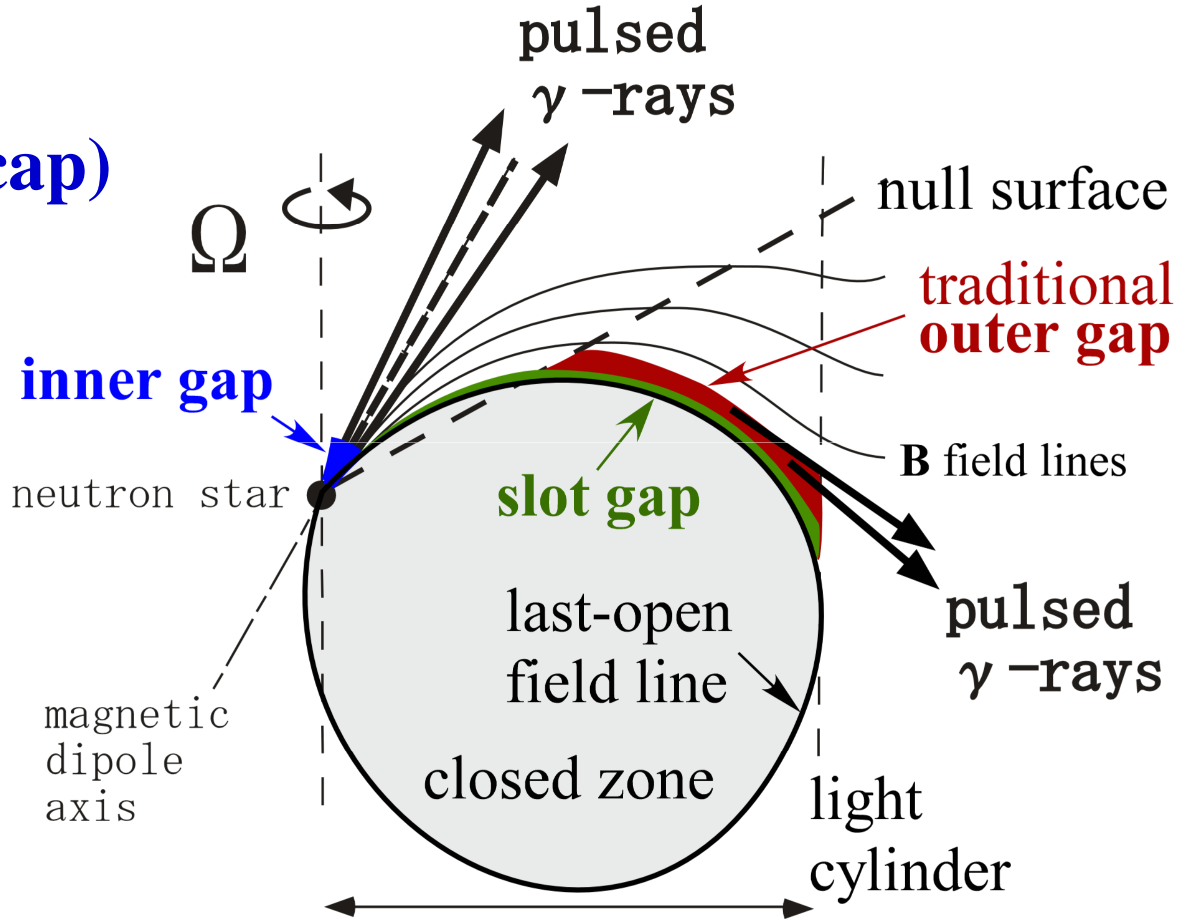

$$\varpi_{LC} = 3\times10^{8}(\Omega/10^{2}\,\mathrm{rad\,s^{-1}})\ \mathrm{cm}$$

§3 Traditional Emission Models

●In traditional IG models, energetics and pair cascade spectrum have had success in reproducing observations.

●However, the predicted beam size is too small to produce the wide pulse profiles that are observed.

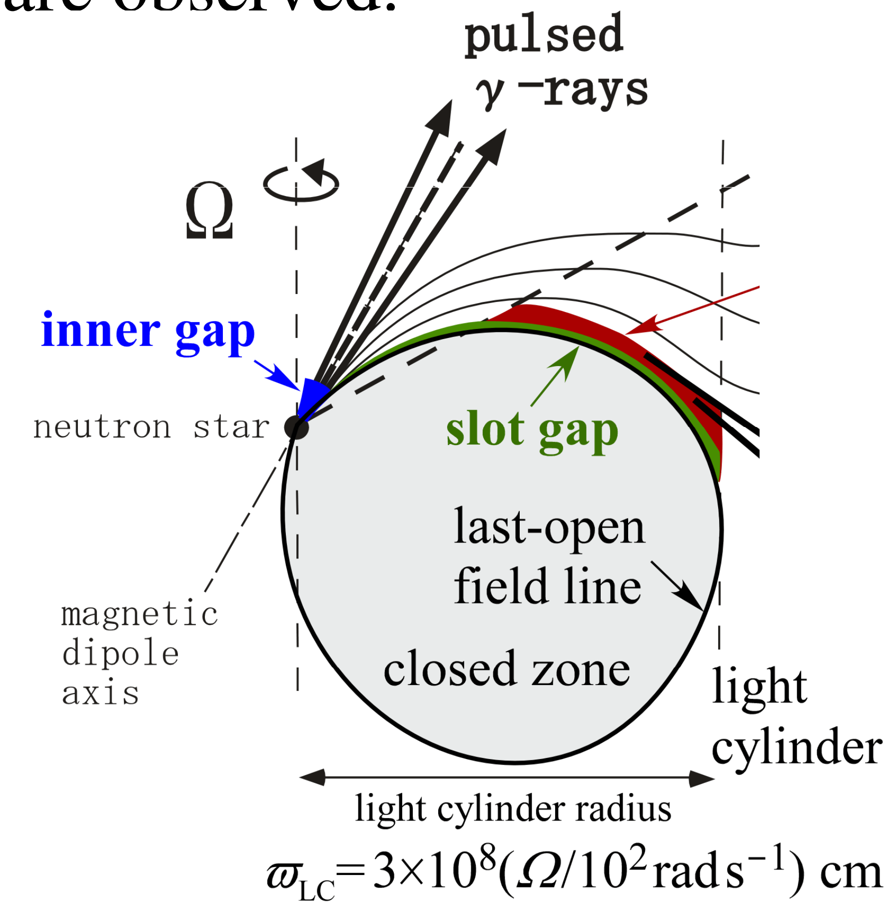

§3 Traditional Emission Models

●In traditional IG models, energetics and pair cascade spectrum have had success in reproducing observations.

●However, the predicted beam size is too small to produce the wide pulse profiles that are observed.

●Arons (1983) first considered high-altitude acceleration region along the last-open field lines: slot-gap model (to consider emission from NS surface to the outer magnetosphere).

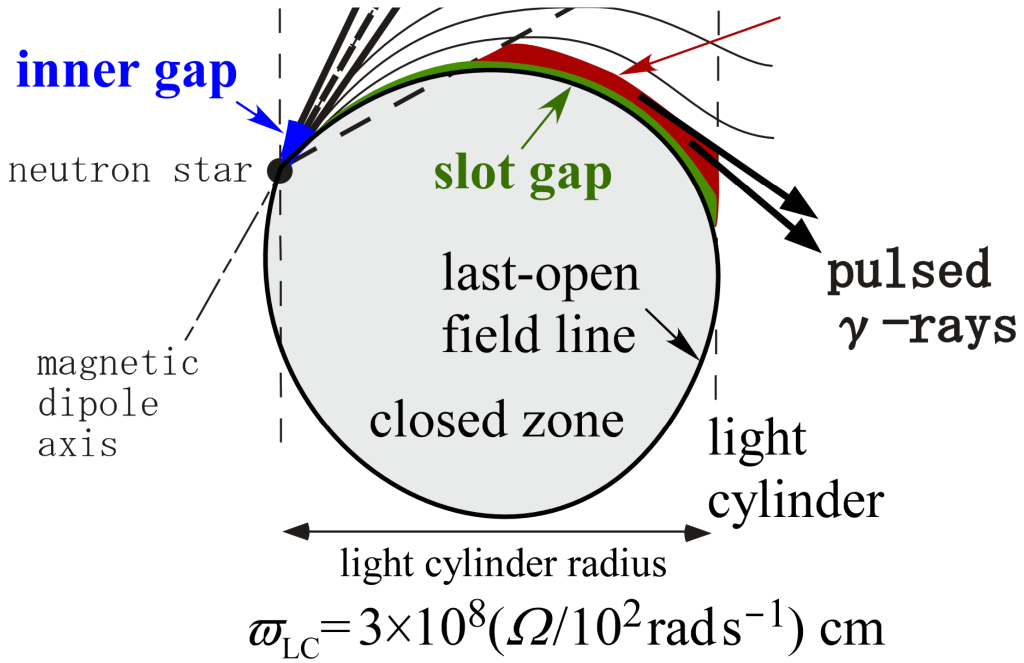

§3 Traditional Emission Models

- In traditional IG models, energetics and pair cascade spectrum have had success in reproducing observations.
- However, the predicted beam size is too small to produce the wide pulse profiles that are observed.
- Arons (1983) first considered high-altitude acceleration region along the last-open field lines: slot-gap model
- Muslimov & Harding ('03; '04) and Dyks, Harding & Rudak ('04) extended the slot-gap model to explain the widely separated double peaks.

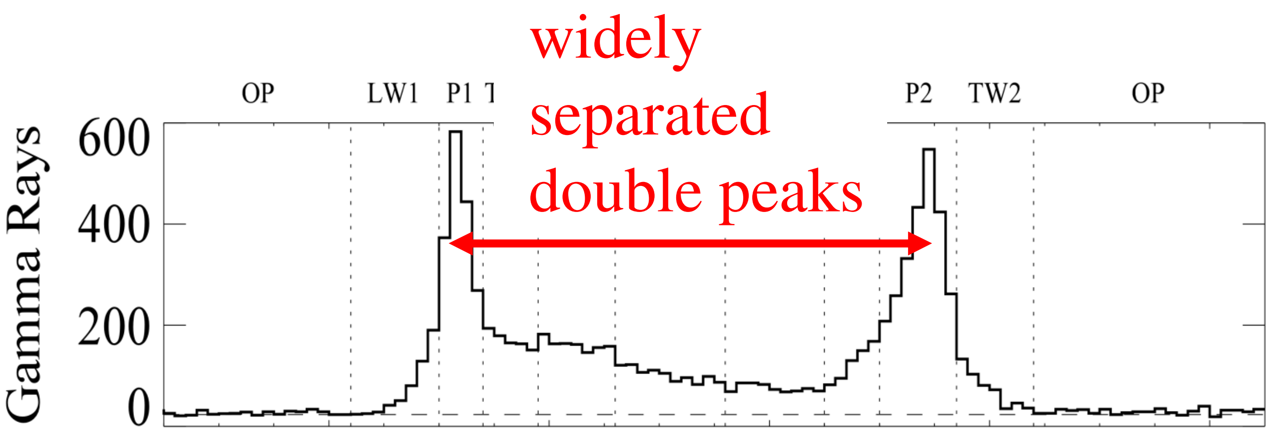

§3 Traditional Emission Models

The OG model provides an alternative possibility.

So far, various properties of high-energy emissions such as double-peak light curves with strong bridges, phase-resolved spectra have been explained with OG models.

Cheng et al. 2000, ApJ 537, 964
Romani 1996, ApJ 470, 469
Chiang & Romani 1994, ApJ 436, 754
Zhang & Cheng 1997, ApJ 487, 370

The purpose of this talk is to re-examine the SG ans OG models (from the first principles) both analytically and numerically and compare their properties.

§4 New Particle Accelerator Theory

In § 5, we analytically investigate the expected γ-ray fluxes from an OG and a SG.

Hirotani (2008, ApJ 688, L25)

In § 6, we numerically re-examine the two models.

Hirotani (2008, Open Astronomy, submitted)

§4 New Gap Theory: Analytical Approach

Since photons are emitted along l.o.s. from interval $2b\rho_c$, the radiative transfer eq. gives the specific intensity,

$$I_\nu \approx 2b\rho_c j_\nu \approx \frac{2}{\pi}\frac{\rho_c}{b} N \frac{dP}{d\nu}$$

j_ν: emission coefficient
N: e^+/e^- # density
$b \sim \gamma^{-1}$: beaming angle
$dP/d\nu$: rad. power / e^-
ρ_c: curvature radius of $\boldsymbol{B}$

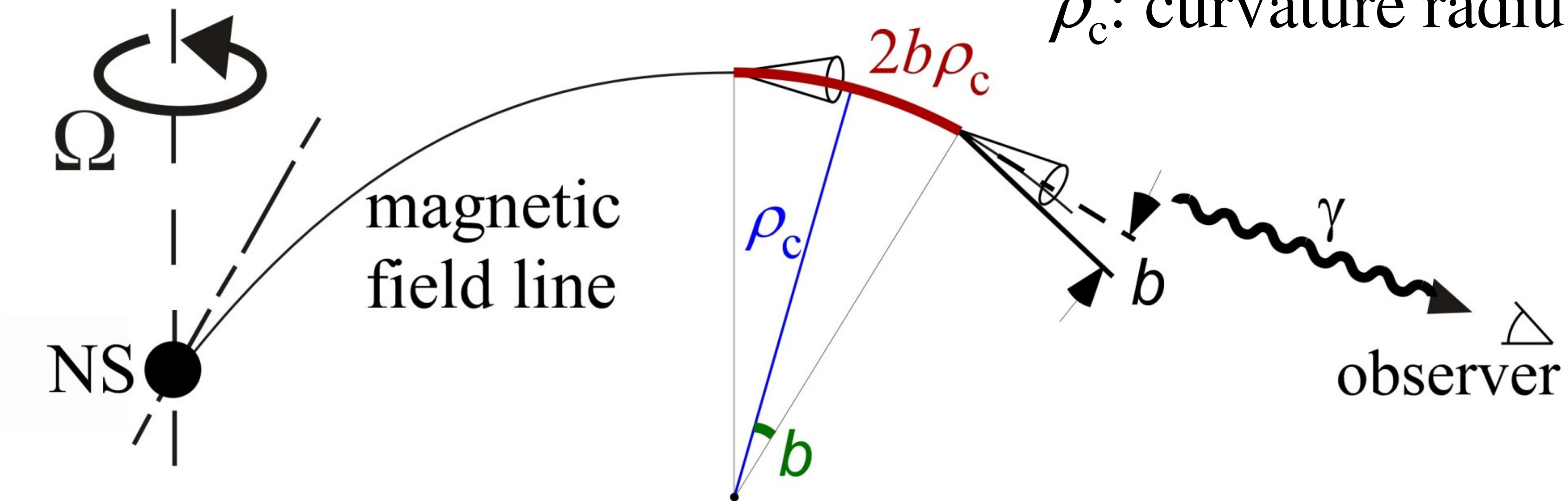

§4 New Gap Theory: Analytical Approach

Since photons are emitted along l.o.s. from interval $2b\rho_c$, the radiative transfer eq. gives the specific intensity,

$$I_\nu \approx 2b\rho_c j_\nu \approx \frac{2}{\pi}\frac{\rho_c}{b} N \frac{dP}{d\nu}$$

For curvature radiation, electrostatic force balance gives

$$\nu \frac{dP}{d\nu} = \frac{9\sqrt{3}}{8\pi} ceE_{\|} \left(\frac{\nu}{\nu_c}\right)^2 \int_{\nu/\nu_c}^{\infty} K_{5/3}(\xi) d\xi$$

$$\nu_c \equiv \frac{3}{4\pi}\frac{c\gamma^3}{\rho_c}: \text{ characteristic freq. of curvature rad.}$$

§4 New Gap Theory: Analytical Approach

Since photons are emitted along l.o.s. from interval $2b\rho_c$, the radiative transfer eq. gives the specific intensity,

$$I_\nu \approx 2b\rho_c j_\nu \approx \frac{2}{\pi}\frac{\rho_c}{b} N \frac{dP}{d\nu}$$

For curvature radiation, electrostatic force balance gives

$$\nu \frac{dP}{d\nu} = \frac{9\sqrt{3}}{8\pi} ceE_\parallel \left(\frac{\nu}{\nu_c}\right)^2 \int_{\nu/\nu_c}^{\infty} K_{5/3}(\xi)d\xi.$$

In a meridionally thin gap ($f \ll 1$),

$$E_\parallel \approx \frac{f^2}{4}\left(\frac{r_*}{\varpi_L}\right)^3 B_* \underbrace{\frac{\partial(-\kappa B_z/B)}{\partial(s/\varpi_L)}}_{\sim 1}$$

B_* : NS surface B

r_*: NS radius

f parameterizes the gap trans-field thickness.

§4 New Gap Theory: Analytical Approach

Using I_ν, we can compute the photon energy flux by

$$\nu F_\nu \approx \nu I_\nu \underbrace{\frac{\Delta A}{d^2}}_{\text{solid angle}}$$

ΔA: area from which photons are emitted toward the observer

d: distance to the emission point

§4 New Gap Theory: Analytical Approach

$$\text{flux:}\quad \nu F_\nu \approx \nu I_\nu \frac{\Delta A}{d^2}, \quad \text{where}\ \ I_\nu \approx \frac{2}{\pi}\frac{\rho_c}{b} N \frac{dP}{d\nu}$$

Cross section from which γ-rays come into l.o.s.:

$$\Delta A \approx \Delta z \times 2br\sin\theta$$

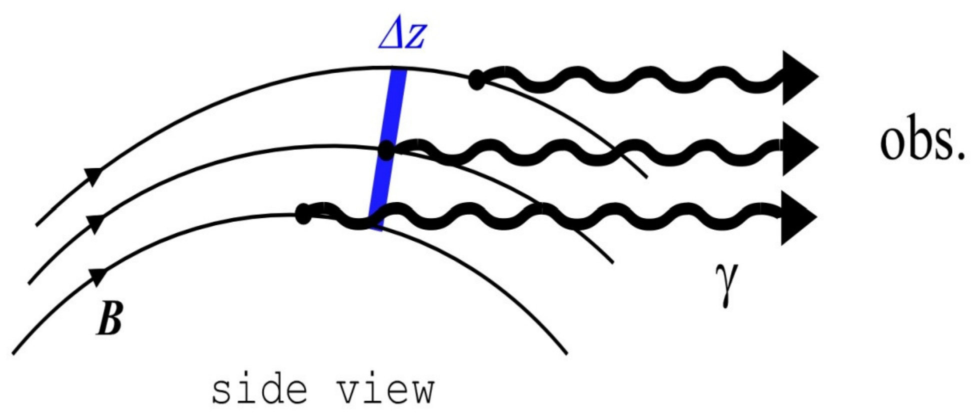

For dipole field,

$$\Delta z \approx 2f \frac{\varpi_L (r/\varpi_L)^2}{\sin\theta\sqrt{1+3\cos^2\theta}}$$

f : gap meridional thickness

f =1: gap exists along all open ***B*** lines

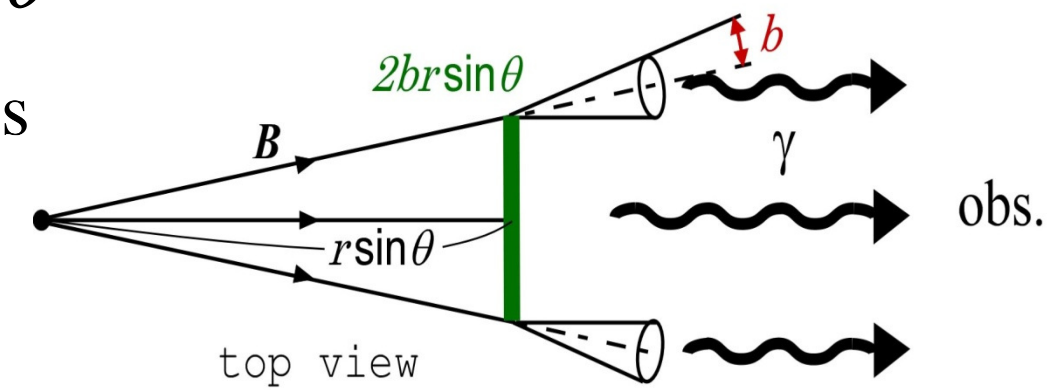

§4 New Gap Theory: Analytical Approach

flux: $\nu F_\nu \approx \nu I_\nu \dfrac{\Delta A}{d^2}$, where $I_\nu \approx \dfrac{2}{\pi}\dfrac{\rho_c}{b} N \dfrac{dP}{d\nu}$

Cross section from which γ-rays come into l.o.s.:

$$\Delta A \approx \Delta z \times 2br\sin\theta$$

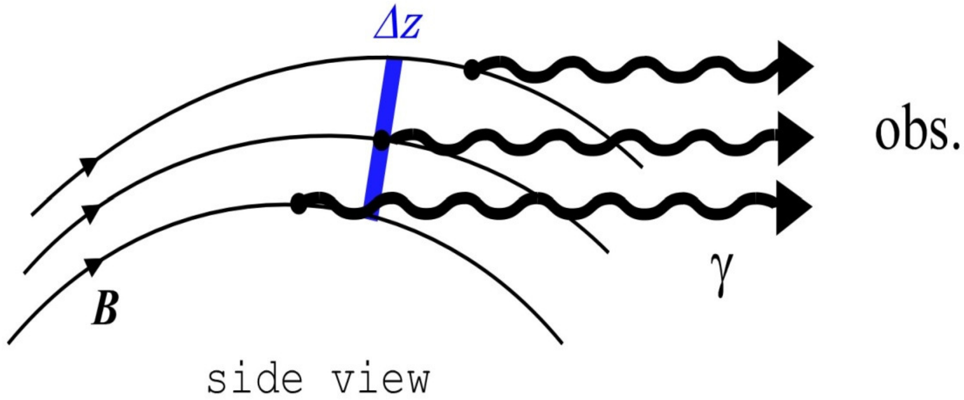

For dipole field,

$$\Delta z \approx 2f \frac{\varpi_L (r/\varpi_L)^2}{\sin\theta\sqrt{1+3\cos^2\theta}}$$

gives

$$\Delta A \approx 2bf\varpi_L^2 \left(\frac{B_*}{B}\right)\left(\frac{r_*}{\varpi_L}\right)^3$$

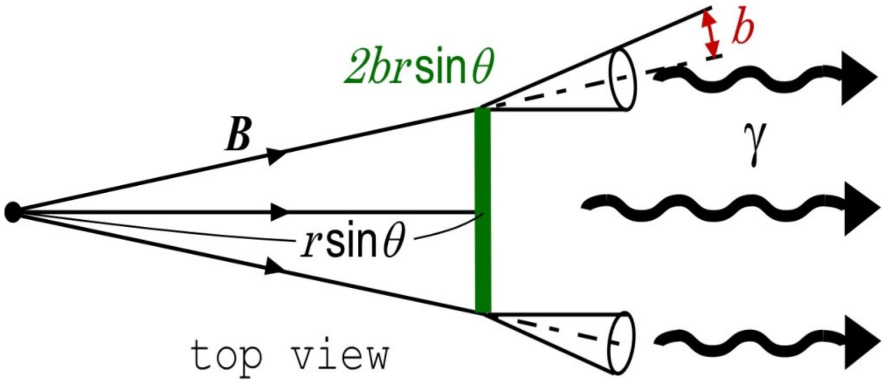

§4 New Gap Theory: Analytical Approach

We finally obtain the photon energy flux at the spectral peak,

$$(\nu F_\nu)_{\rm peak} \approx 0.0450 f^3 \kappa \underbrace{\frac{\mu^2 \Omega^4}{c^3} \frac{1}{d^2}}_{\propto \dot{E}/d^2 \,:\ \text{spin-down flux}}, \qquad \kappa \sim 1.$$

f: fractional gap width ($f \ll 1$ denotes a thin gap)

It was, therefore, natural that only the highest-spin-down pulsars have been detected with EGRET.

The difference between OG and SG models appears through f, κ, and assumed μ (magnetic moment).

§4 New Gap Theory: Analytical Approach

$$(\nu F_\nu)_{\rm peak} \approx 0.0450 f^3 \kappa \frac{\mu^2 \Omega^4}{c^3} \frac{1}{d^2}$$

Apply this general result to the Crab pulsar (Ω=190 rad s^{-1}).

Hirotani (2008) ApJ 688, L25

(I) For OG model (f~0.14, κ~0.3, μ=4×10^{30} G cm^3),

$(\nu F_\nu)_{\rm peak} \sim 4\times10^{-4}$ MeV s^{-1} cm^{-2} ~ EGRET flux.

(II) For SG model (f~0.04, κ~0.2), even with a large μ,

$(\nu F_\nu)_{\rm peak} \sim 3\times10^{-5} (\mu/8\times10^{30})^2$ MeV s^{-1} cm^{-2}

< 0.1 EGRET flux.

Unfortunately, Harding + ('08, ApJ 680, 1378) overestimated the flux more than 5 times because of a programming bug.

§4 New Gap Theory: Analytical Approach

We will confirm these analytical conclusions
by numerical computations in the next section.

Apply this general result to the Crab pulsar (Ω=190 rad s^{-1}).

Hirotani (2008) ApJ 688, L25

(I) For OG model (f~0.14, κ~0.3, μ=4×10^{30} G cm^3),

$(\nu F_\nu)_{peak} \sim 4\times10^{-4}$ MeV s^{-1} cm^{-2} ~ EGRET flux.

(II) For SG model (f~0.04, κ~0.2), even with a large μ,

$(\nu F_\nu)_{peak} \sim 3\times10^{-5} (\mu/8\times10^{30})^2$ MeV s^{-1} cm^{-2}

< 0.1 EGRET flux.

§5 New Gap Theory: Numerical Approach

A stationary, self-sustained pair-production cascade in a rotating NS magnetosphere:

$e^{\pm}$'s are accelerated by $E_{\parallel}$

↓

Relativistic e^+/e^- emit γ-rays via synchro-curvature, and IC processes

↓

γ-rays collide with soft photons/B to materialize as pairs in the accelerator

§5 New Gap Theory: Numerical Approach

The Poisson equation for the electrostatic potential ψ is given by

$$-\nabla^2 \psi = 4\pi(\rho - \rho_{\mathrm{GJ}}) \ ,$$

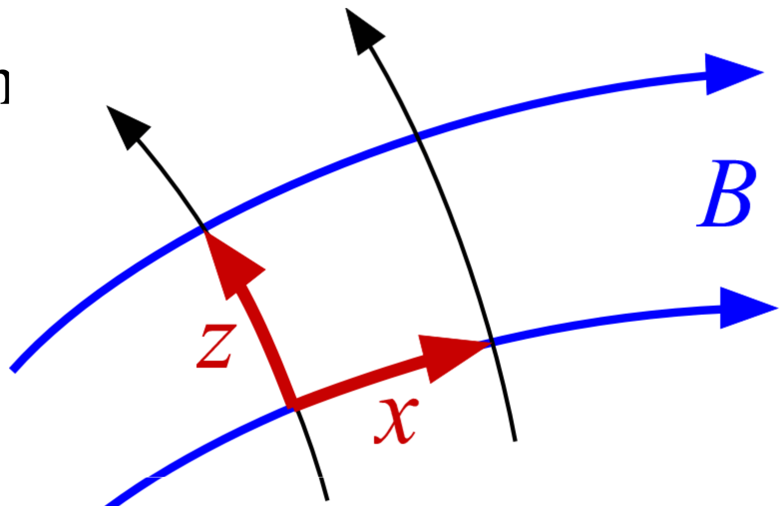

where $E_{\parallel} \equiv -\dfrac{\partial \Psi}{\partial x}$,

$$\rho \equiv e \int_0^\infty d\Gamma \left[N_+(x,z,\Gamma) - N_-(x,z,\Gamma) \right] + \rho_{\mathrm{ion}} \ ,$$

$$\rho_{\mathrm{GJ}} \equiv -\frac{\mathbf{\Omega} \bullet \mathbf{B}}{2\pi c} \ .$$

N_+ / N_-: distrib. func. of e^+/e^-

Γ: Lorentz factor of e^+/e^-

§5 New Gap Theory: Numerical Approach

Assuming $\partial_t + \Omega\partial_\phi = 0$, we solve the $e^{\pm}$'s Boltzmann eqs.

$$\frac{\partial N_{\pm}}{\partial t} + \vec{v}\cdot\nabla N_{\pm} + \left(e\vec{E}_{\parallel} + \frac{\vec{v}}{c}\times\vec{B} \right)\cdot\frac{\partial N_{\pm}}{\partial \vec{p}} = S_{IC} + \int \alpha_\nu d\nu \int \frac{I_\nu}{h\nu} d\omega$$

together with the radiative transfer equation,

$$\frac{dI_\nu}{dl} = -\alpha_\nu I_\nu + j_\nu$$

$N_{\pm}$: positronic/electronic spatial # density,
$E_{\parallel}$: mangnetic-field-aligned electric field,
S_{IC}: ICS re-distribution function, $d\omega$: solid angle element,
I_ν: specific intensity, l : path length along the ray
α_ν: absorption coefficient, j_ν: emission coefficient

§5 New Gap Theory: Numerical Approach

Specify the three parameters: (period, P, is known.)

- magnetic inclination (e.g., $\alpha_{\rm inc}$=45°, 75°),
- magnetic dipole moment of NS (e.g., $\mu=4\times10^{30}\,\mathrm{G\,cm^3}$)
- neutron-star surface temperature (e.g., $kT_{\rm NS}$=50 eV)

Solve Poisson eq. + Boltzmann eqs. in 6-D phase space (i.e., 3-D config. + 3-D mom. space) + RTE.

I first solved (Hirotani '08, Open Astron., submitted)

- gap geometry,
- acceleration electric field distribution,
- particle density and energy spectrum,
- γ-ray flux and energy spectrum,

by specifying these three parameters.

§5 New Gap Theory: Numerical Approach

I applied the theory to the Crab pulsar.

§5 New Gap Theory: Numerical Approach

3-D distribution of the particle accelerator (i.e., high-energy emission zone) is solved from the Poisson eq.

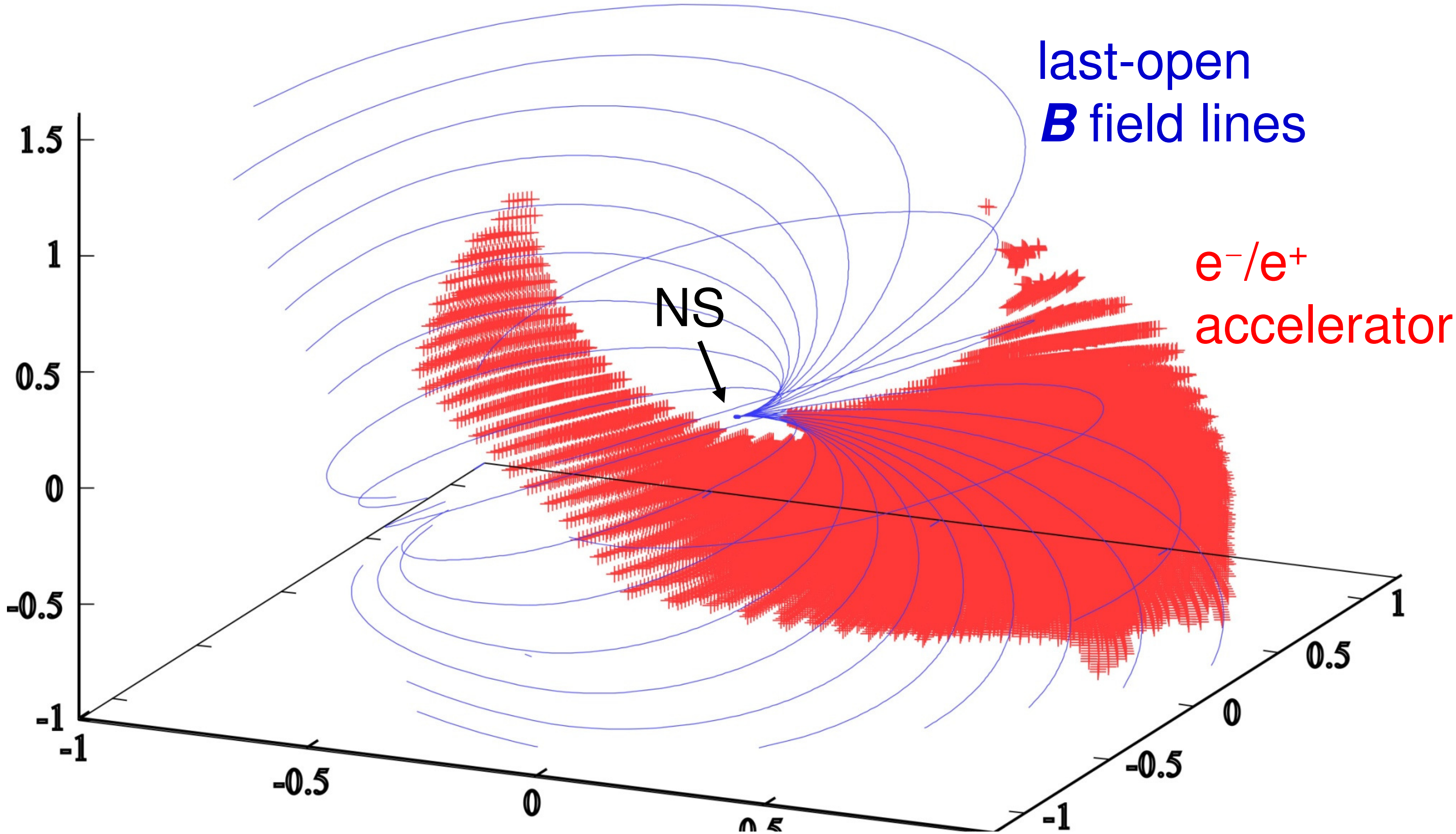

§5 New Gap Theory: Numerical Approach

The gap activity is controlled by f^3.

meridional thickness, $f = f(s, \phi)$. [ϕ: magnetic azimuth]

- Previous models: assume or estimate f by dim. analysis.
- This work: solve f from the basic eqs. in 3-D mag. sphere.

Fig.) gap trans-field thickness on 2-D last-open-field-line surface

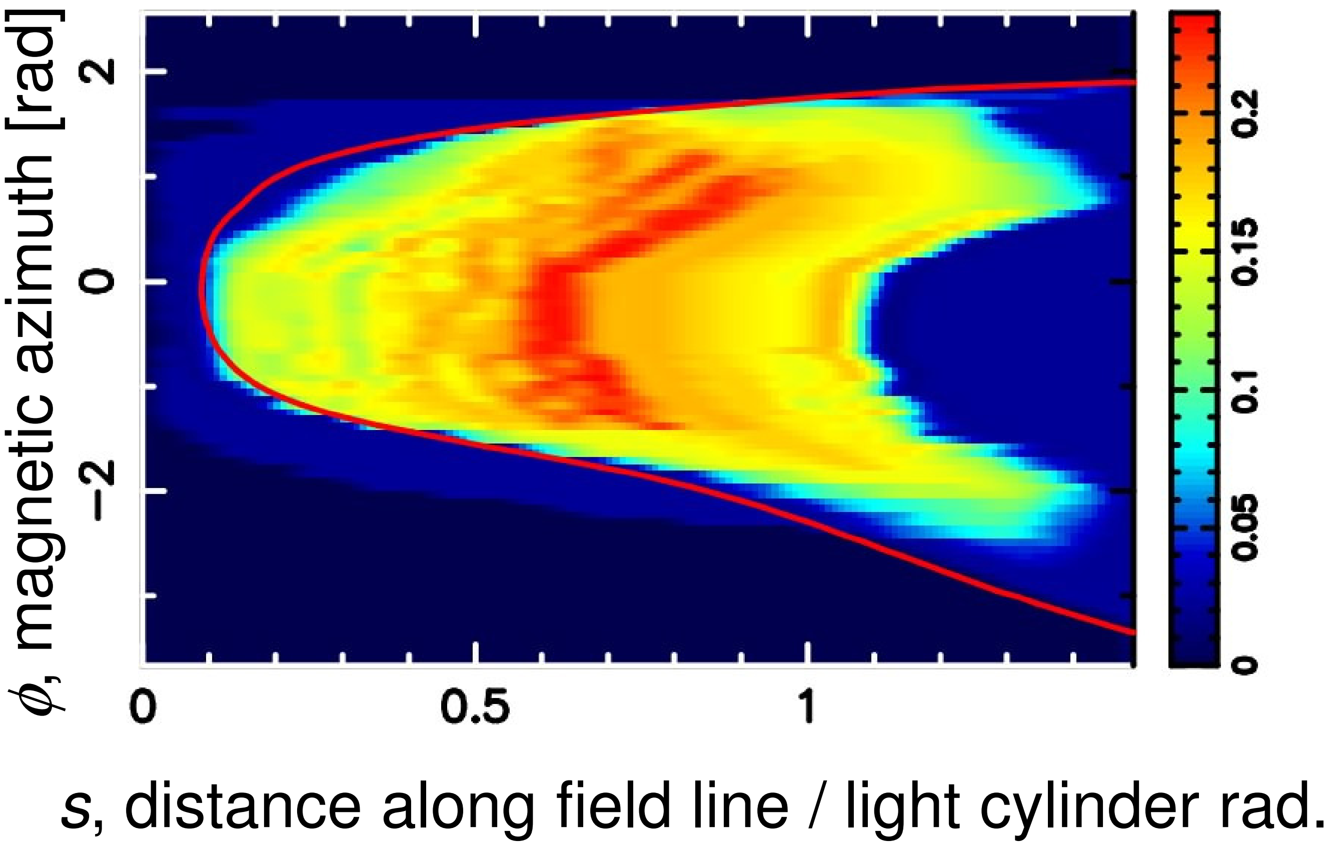

§5 New Gap Theory: Numerical Approach

Intrinsic quantities (e.g., gap 3-D geometry, f, $E_{\|}$, $e^{\pm}$ distribution functions, specific intensity at each point) of an OG is self-consistently solved if we give ***B*** inclination, NS magnetic moment, NS surface temperature, without introducing any artificial assumptions.

If we additionally give the distance and observer's viewing angle, we can predict the luminosity, pulse profiles, and the photon spectrum in each pulse phase.

§5 New Gap Theory: Numerical Approach

Photons are emitted along the local ***B*** field lines (in the co-rotating frame) by relativistic beaming and propagate in a hollow cone.

The hollow cone emission is projected on the 2-D propagation directional plane.

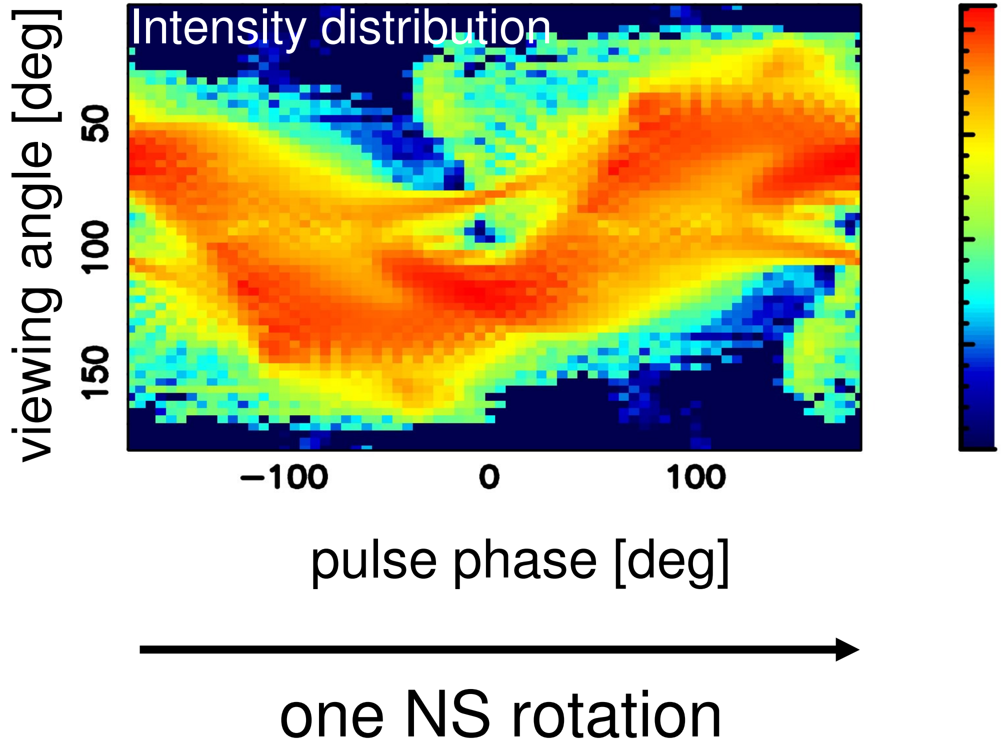

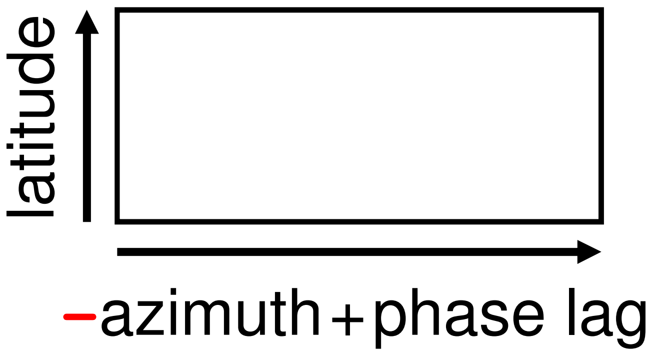

Photons emitted at smaller azimuth arrives earlier.

§5 New Gap Theory: Numerical Approach

Photons are emitted along the local ***B*** field lines (in the co-rotating frame) by relativistic beaming and propagate in a hollow cone.

The hollow cone emission is projected on the 2-D propagation directional plane.

If we specify the observer's viewing angle, we obtain the pulse profile.

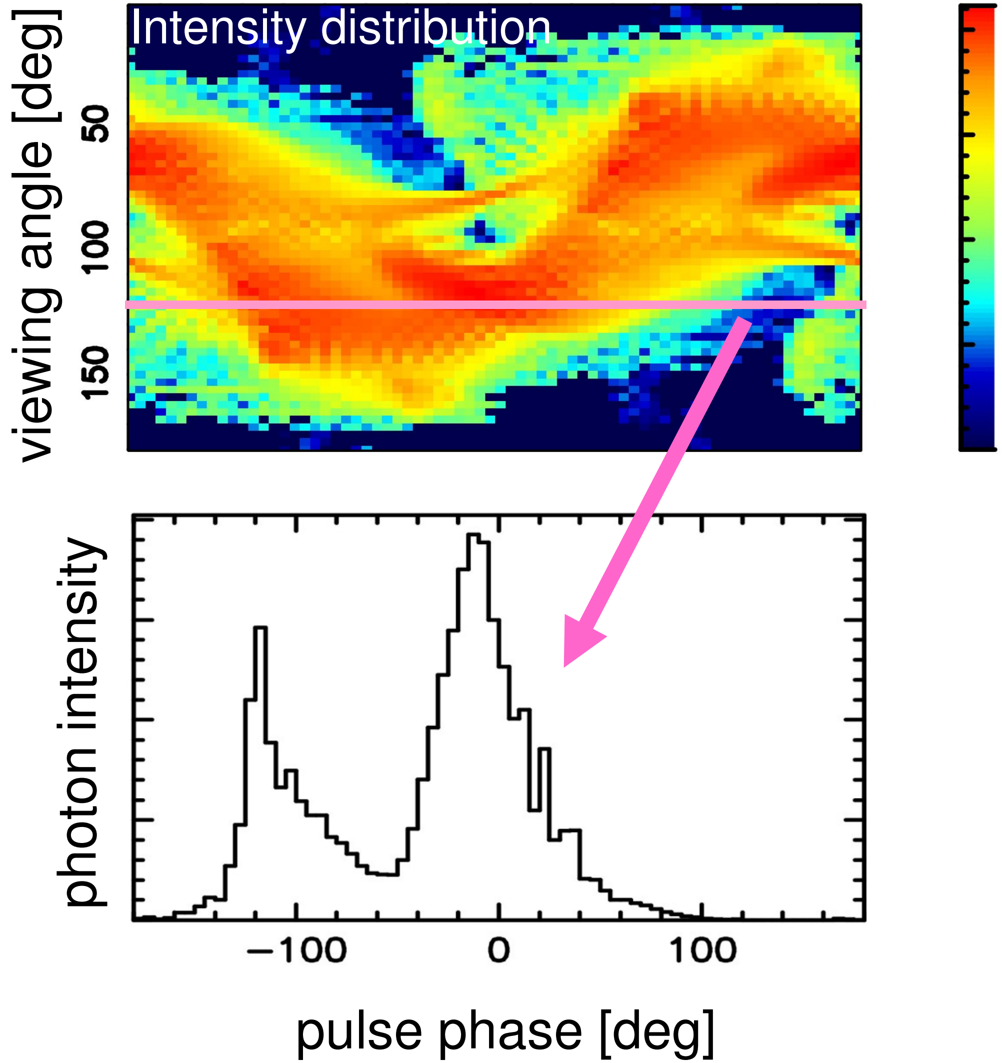

§5 New Gap Theory: Numerical Approach

Predicted spectra reproduce observations, if we assume appropriate viewing angle (e.g., ~100°).

Fig.) OG prediction of Crab νF_ν spectra

solid:
un-abs. primary

dashed:
un-abs. 2ndary

red:
to be observed,
prim.+2nd+3rd

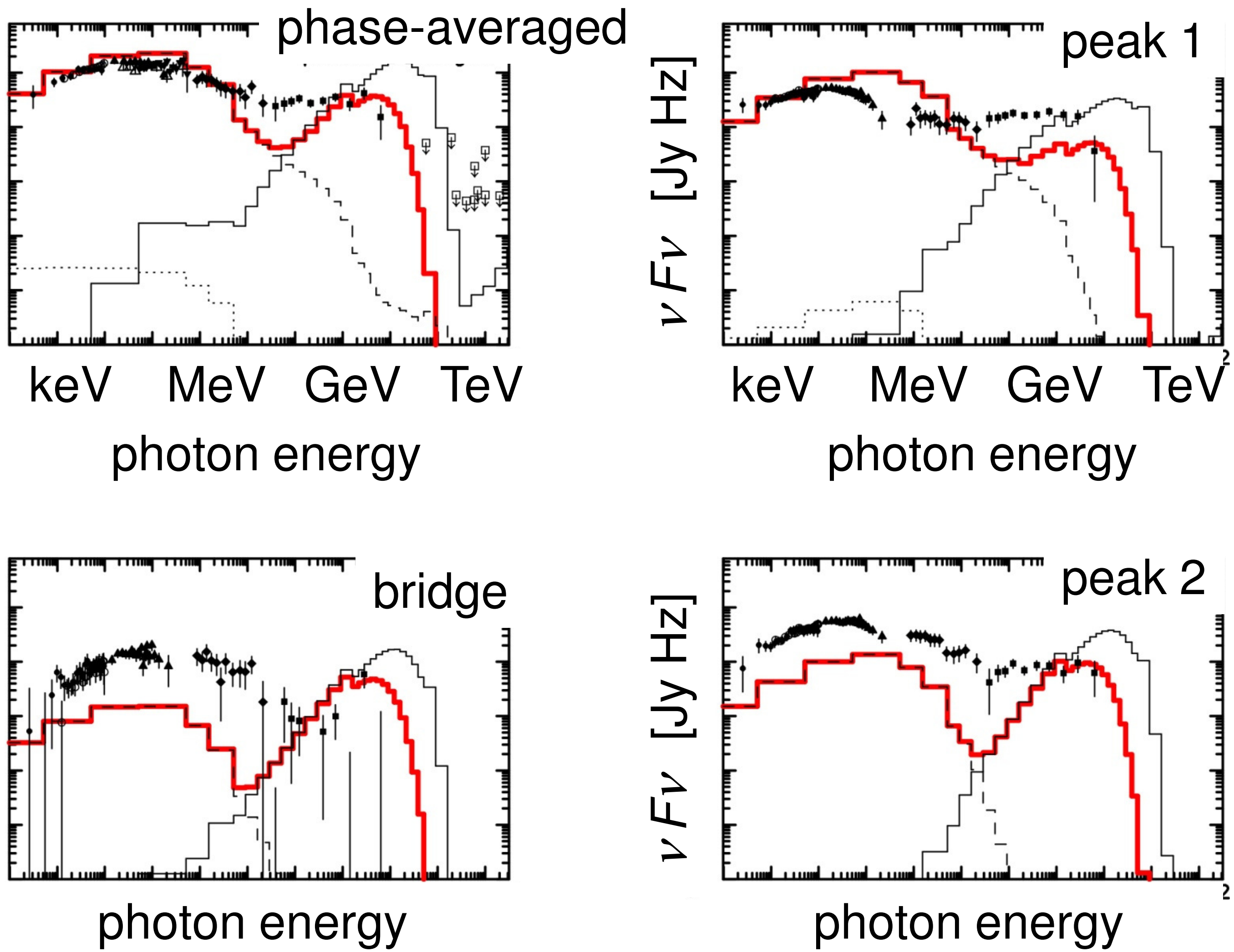

§5 New Gap Theory: Numerical Approach

Another example: the case of the CTA 1 pulsar

About 3 times smaller flux than Fermi's.

ICS component may be detected above TeV.

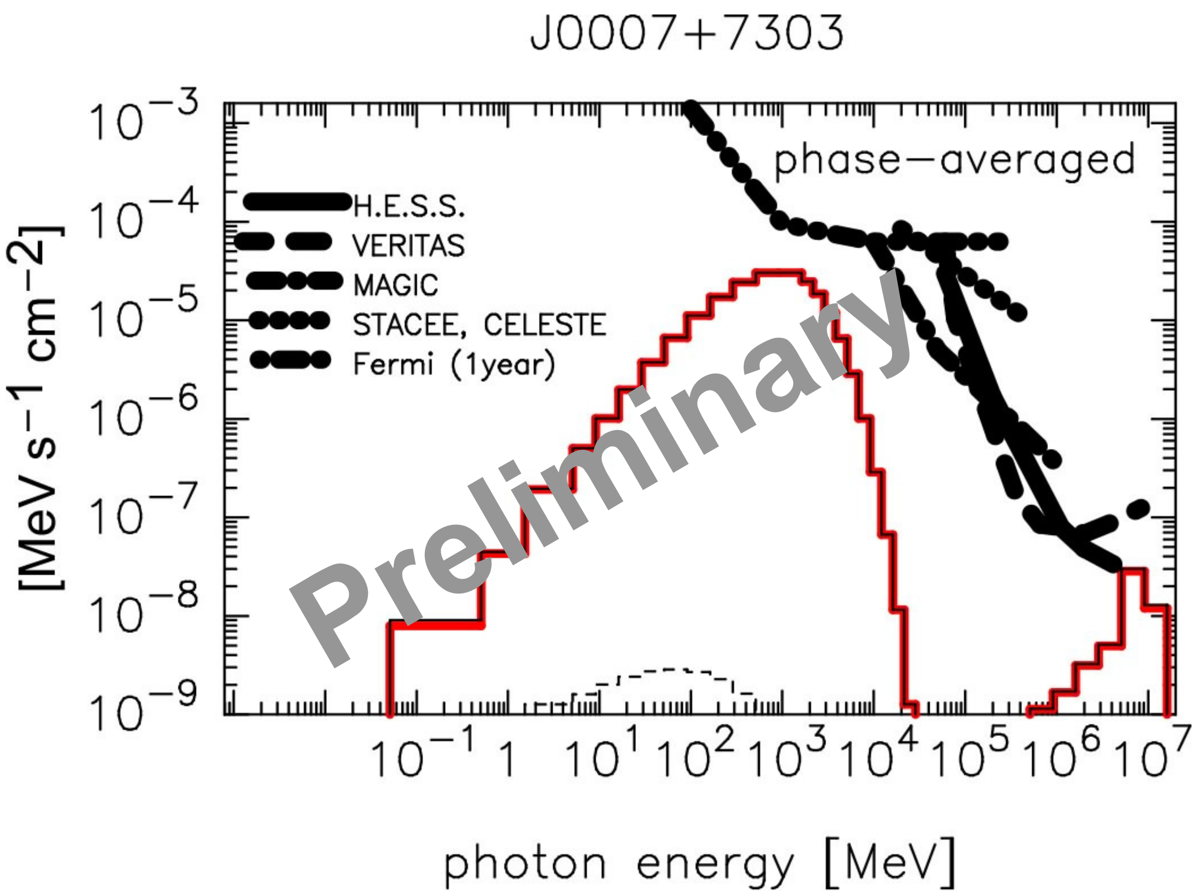

Fig. Phase-averaged spectrum of CTA1 pulsar at viewing angles=100°.

§5 *New Gap Theory: Numerical Approach*

In short, the solution (coincidentally) corresponds to a quantitative extension of the previous OG model. The solution is roughly consistent with observations.

How about the SG model?

To obtain the solution that corresponds to the SG model, we must introduce two additional assumptions:

(1) give f (e.g., ~0.04), instead of solve it.
(2) modify the Goldreich-Julian charge density by hand

geometrically defined from the first principles;
thus, cannot be modified conveniently…

§5 New Gap Theory: Numerical Approach

The Slot-gap model reproduces the pulse profile, as predicted by Harding + (2008).

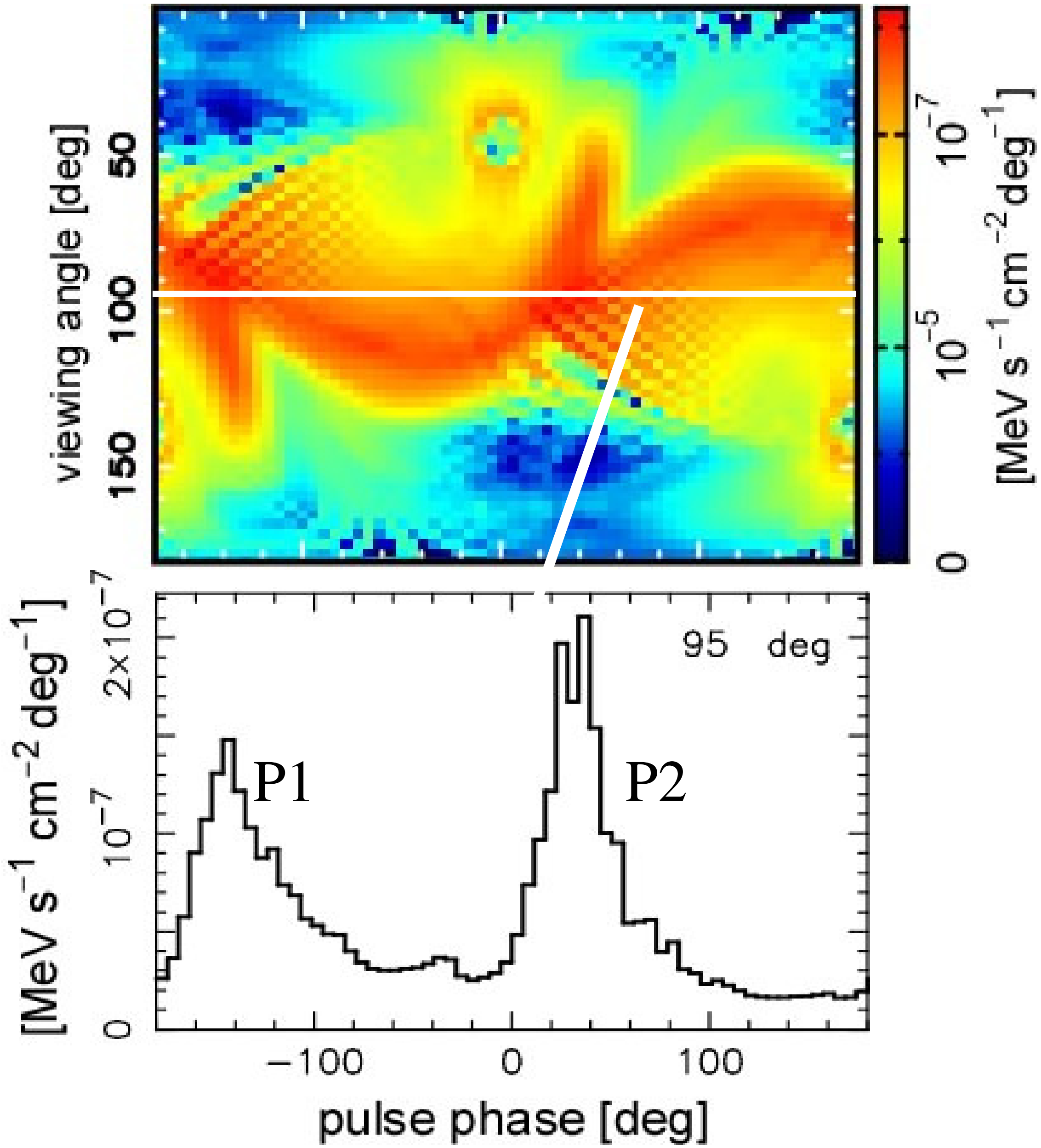

Double peaks are also formed in the SG model.

§5 New Gap Theory: Numerical Approach

The Slot-gap model reproduces the pulse profile, as predicted by Harding + (2008).

However, the predicted photon flux is too small.

Note that this result is consistent with analytic one (§ 5), 2×10^{-5} MeV s^{-1} cm^{-2}.

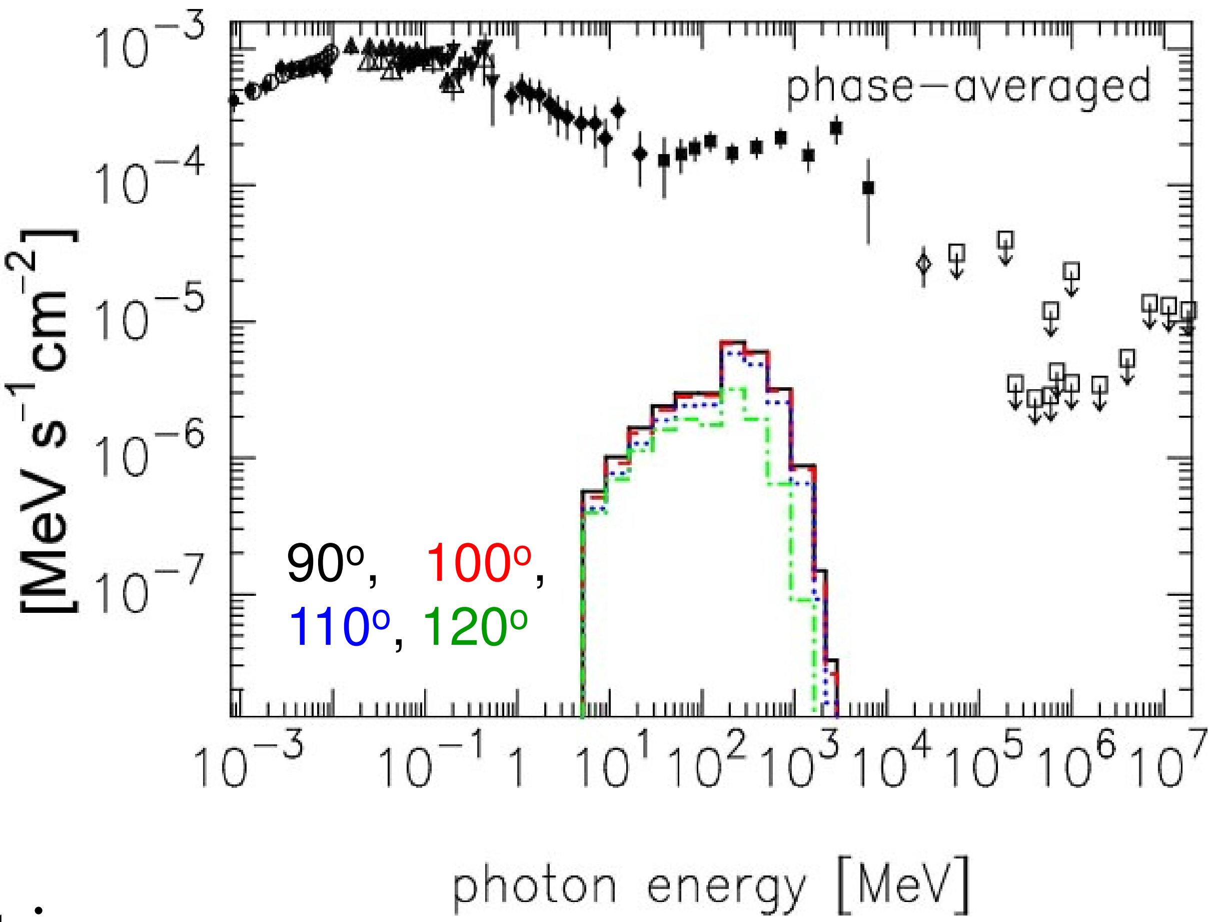

Fig. Phase-averaged SG spectrum for four discrete viewing angles, 90°, 100°, 110°, and 120°.

Summary

- High-energy emissions from pulsar magnetospheres are first solved from the set of Maxwell (div$\boldsymbol{E}=4\pi\rho$ only) and Boltzmann eqs., if we specify P, dP/dt, α_{incl}, kT_{NS}. We no longer have to assume the gap geometry, $E_{\parallel}$, $e^{\pm}$ distribution functions. ($\boldsymbol{B}$ field $\leftarrow$ vacuum rotating dipole solution)

- The obtained solution for the Crab pulsar corresponds to a quantitative extension of the previous, phenomenological OG models, and qualitatively reproduces the observations in IR-VHE.

- SG model can account for less than 10% of the observed Crab γ-ray flux.

- The same scheme can be applied for arbitrary rotation-powered pulsars.

Problematic assumption in SG model

The Goldreich-Julian charge density is uniquely given by the ***B*** field geometry, and not allowed to change it artificially.

$$\rho_{\mathrm{GJ}} \approx -\frac{\mathbf{\Omega}\cdot\mathbf{B}}{2\pi c} \quad \text{(Newtonian)}$$

$$\rho_{\mathrm{GJ}} = \frac{c^2}{4\pi\sqrt{-g}} \partial_\mu \left(\frac{\sqrt{-g}}{\rho_w^2} g^{\mu\nu} g_{\varphi\varphi} \left(\Omega - \omega\right) F_{\varphi\nu} \right) \quad \text{(GR)}$$

It is derived from the first principle, div$\boldsymbol{E}=4\pi\rho$ and the assumption, $F_{\mu t} + \Omega F_{\mu\varphi} = -\partial_\mu \Psi(r,\theta,\varphi - \Omega t)$.

Problematic assumption in SG model

GJ charge density:

$$\rho_{\mathrm{GJ}} = \frac{c^2}{4\pi\sqrt{-g}}\partial_\mu\left(\frac{\sqrt{-g}}{\rho_w^2}g^{\mu\nu}g_{\varphi\varphi}(\Omega-\omega)F_{\varphi\nu}\right).$$

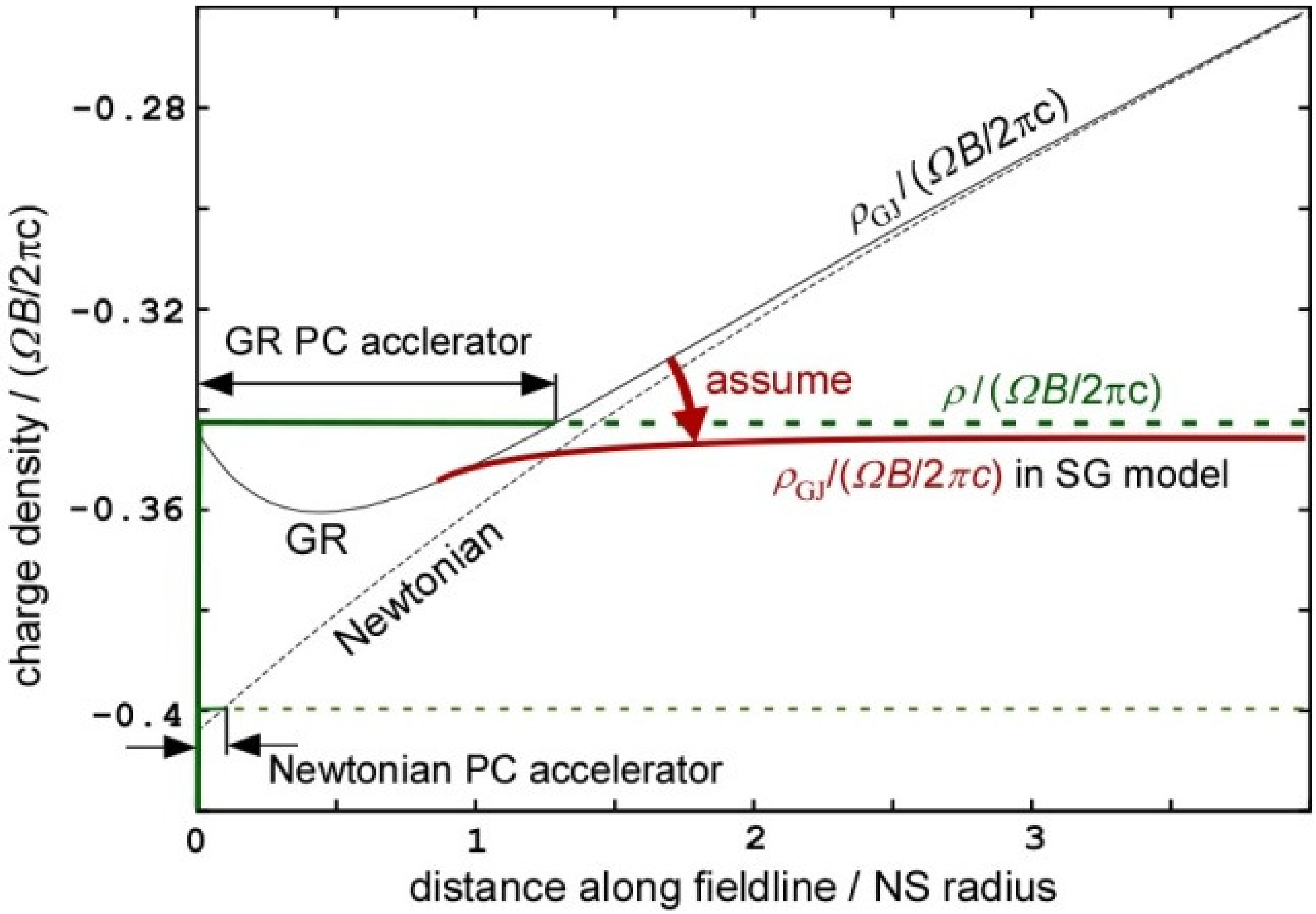

Problematic assumption in SG model

The Goldreich-Julian charge density is uniquely given by the ***B*** field geometry, and not allowed to change it artificially.

$$\rho_{\mathrm{GJ}} \approx -\frac{\mathbf{\Omega} \cdot \mathbf{B}}{2\pi c} \quad \text{(Newtonian)}$$

$$\rho_{\mathrm{GJ}} = \frac{c^2}{4\pi\sqrt{-g}} \partial_\mu \left(\frac{\sqrt{-g}}{\rho_w^2} g^{\mu\nu} g_{\varphi\varphi} (\Omega - \omega) F_{\varphi\nu} \right) \quad \text{(GR)}$$

However, in the SG model, they modify $\rho_{\mathrm{GJ}}/\mathrm{B}$ by hand.

§1 Introduction: The γ-ray sky

The *Large Area Telescope* (20 MeV – 300 GeV) aboard the *Fermi Gamma-Ray Space Telescope*.

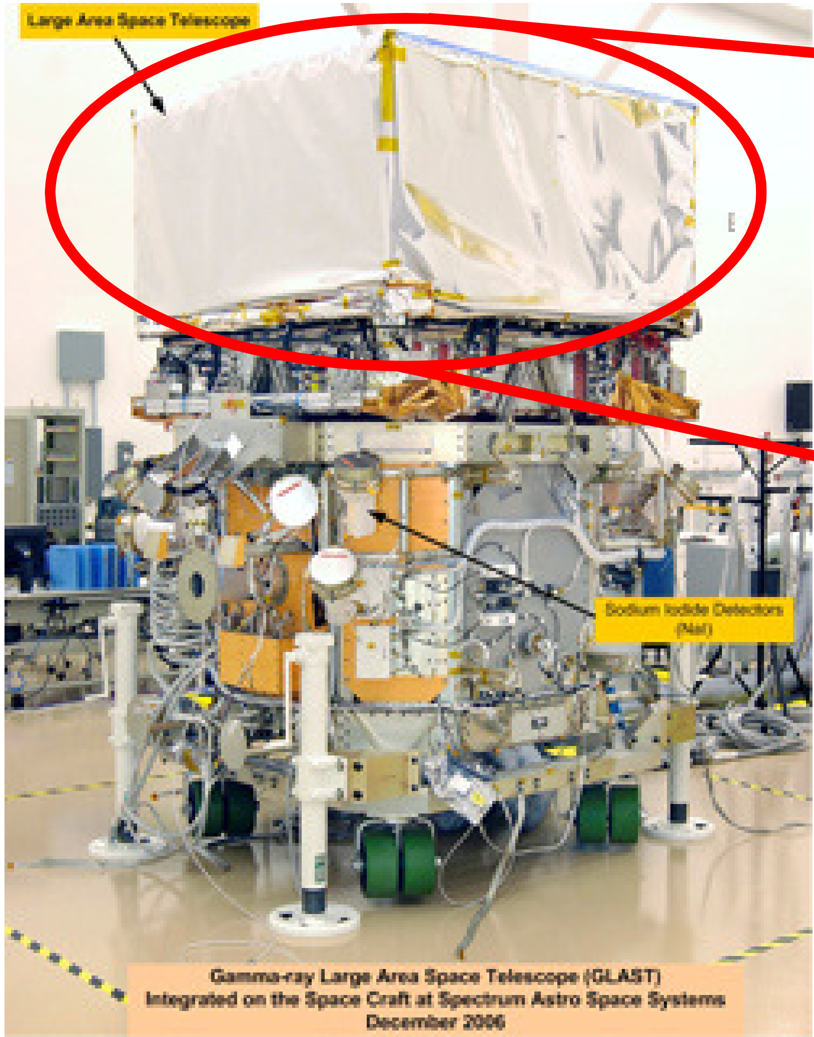

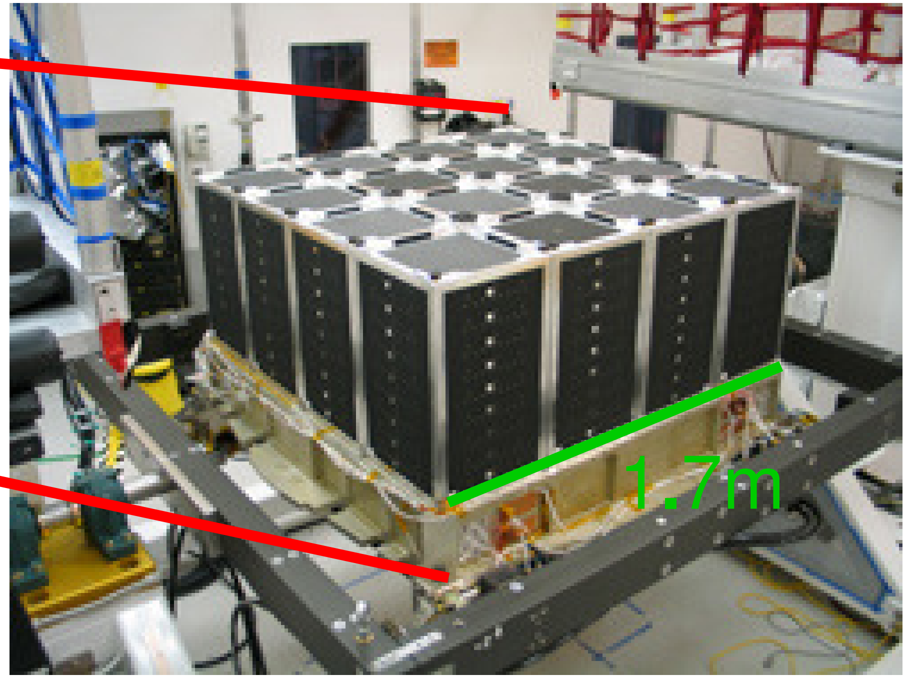

LAT PSF ~ 0.1^o @ 1 GeV
FOV ~ 2.5 ster
sensitivity ~ 30*EGRET

§1 Introduction: The γ-ray sky

The *Large Area Telescope* (20 MeV – 300 GeV) aboard the *Fermi Gamma-Ray Space Telescope*.

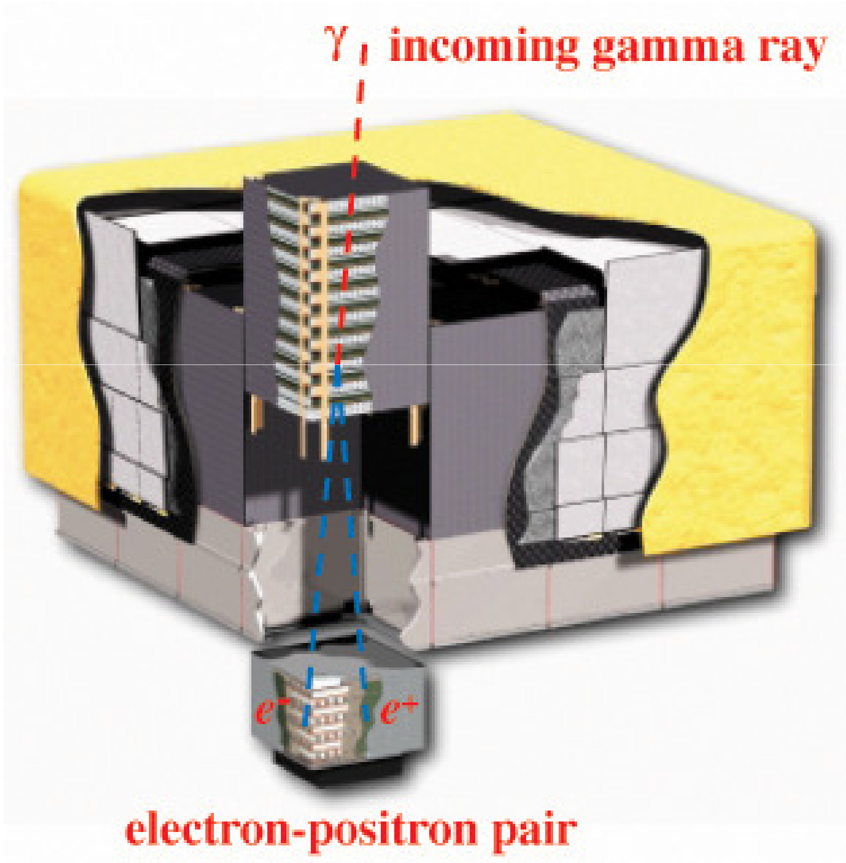

§2 γ-ray Observations of Pulsars

Pulsars are the most luminous objects in the γ-ray sky.

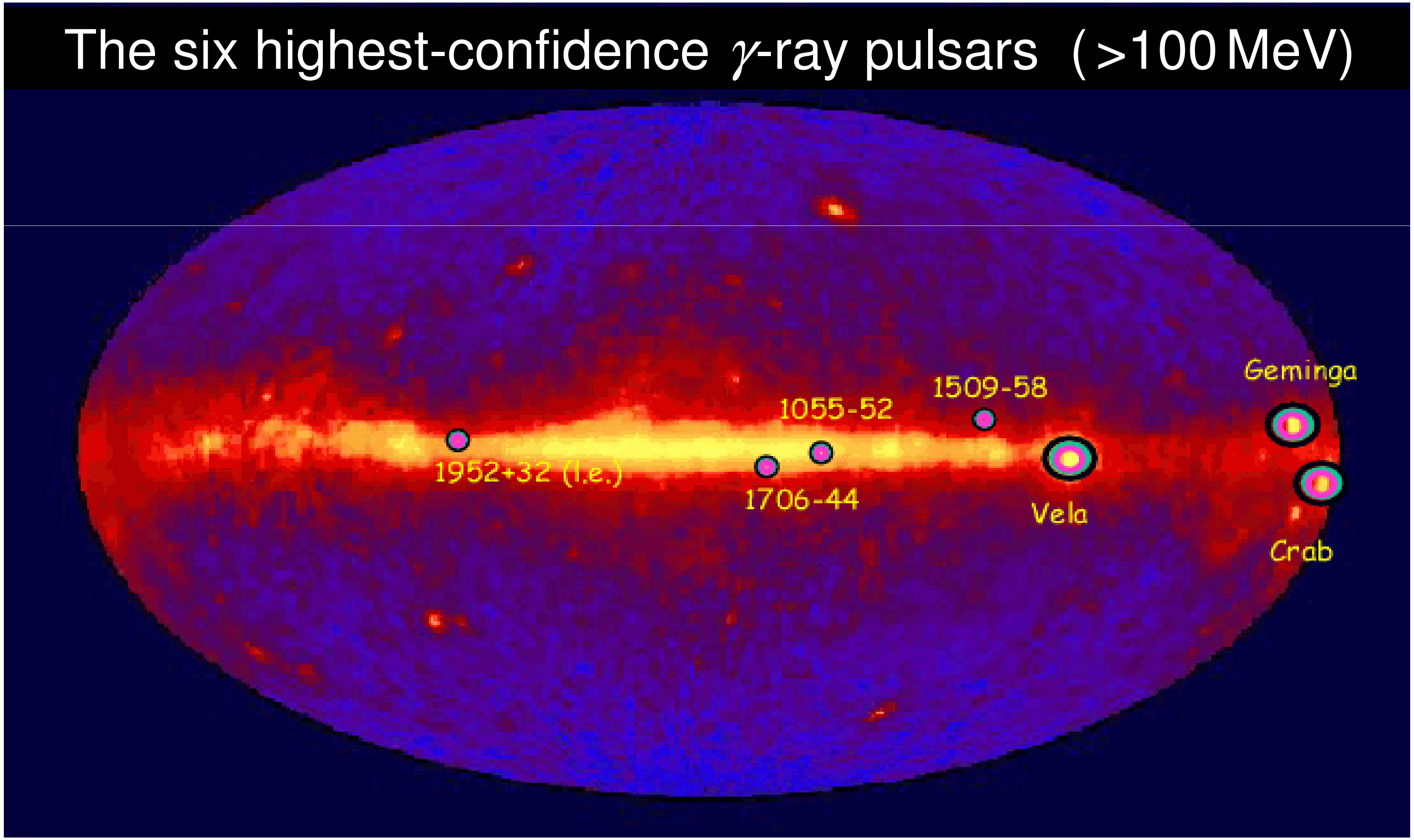

§1 Introduction: CGRO observations

γ-ray pulsars emit radiation in a wide frequency range:

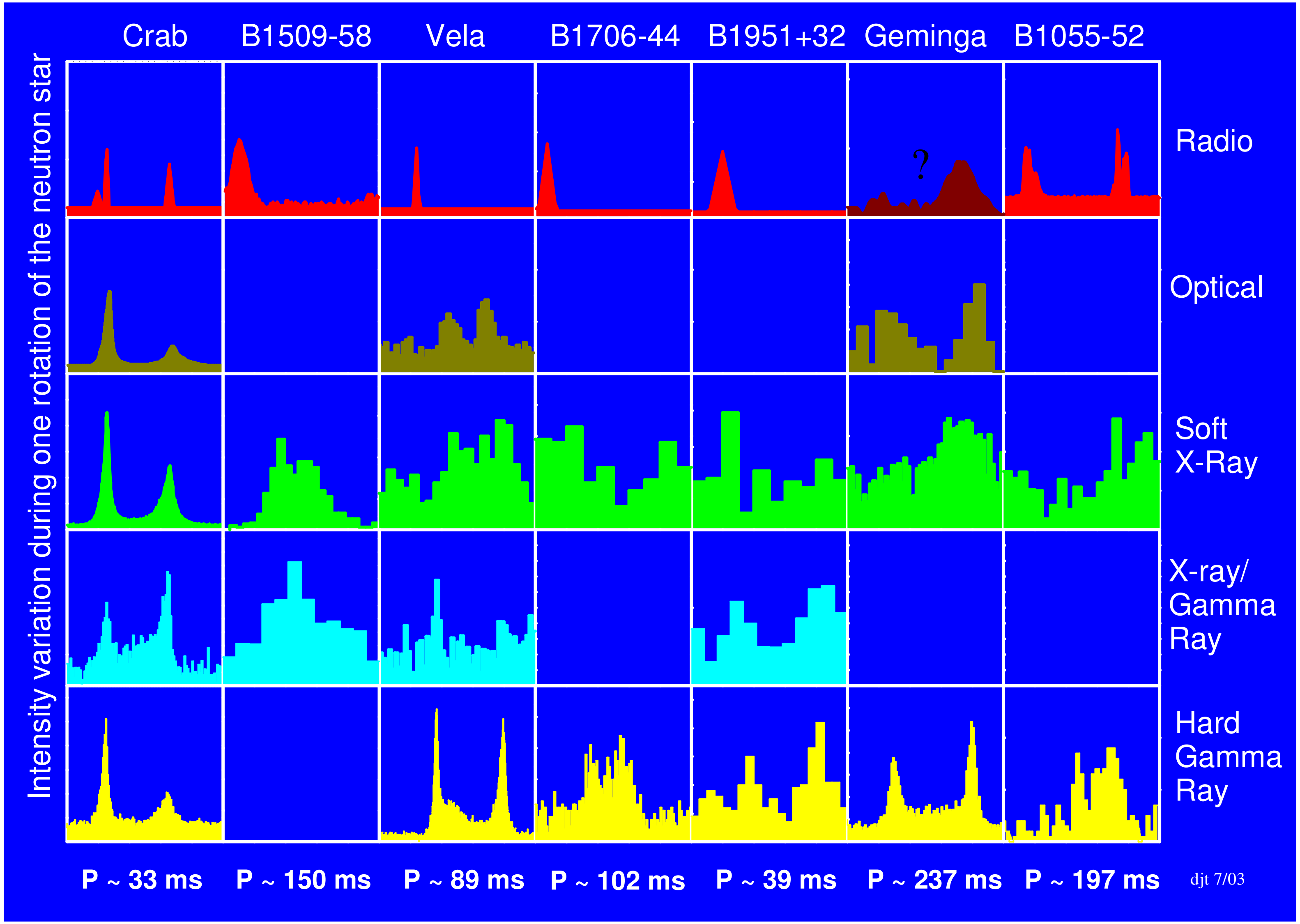

Thompson 2003, astro-ph/0312272

Compton Gamma Ray Observatory

Light curves: total vs. hard γ-rays

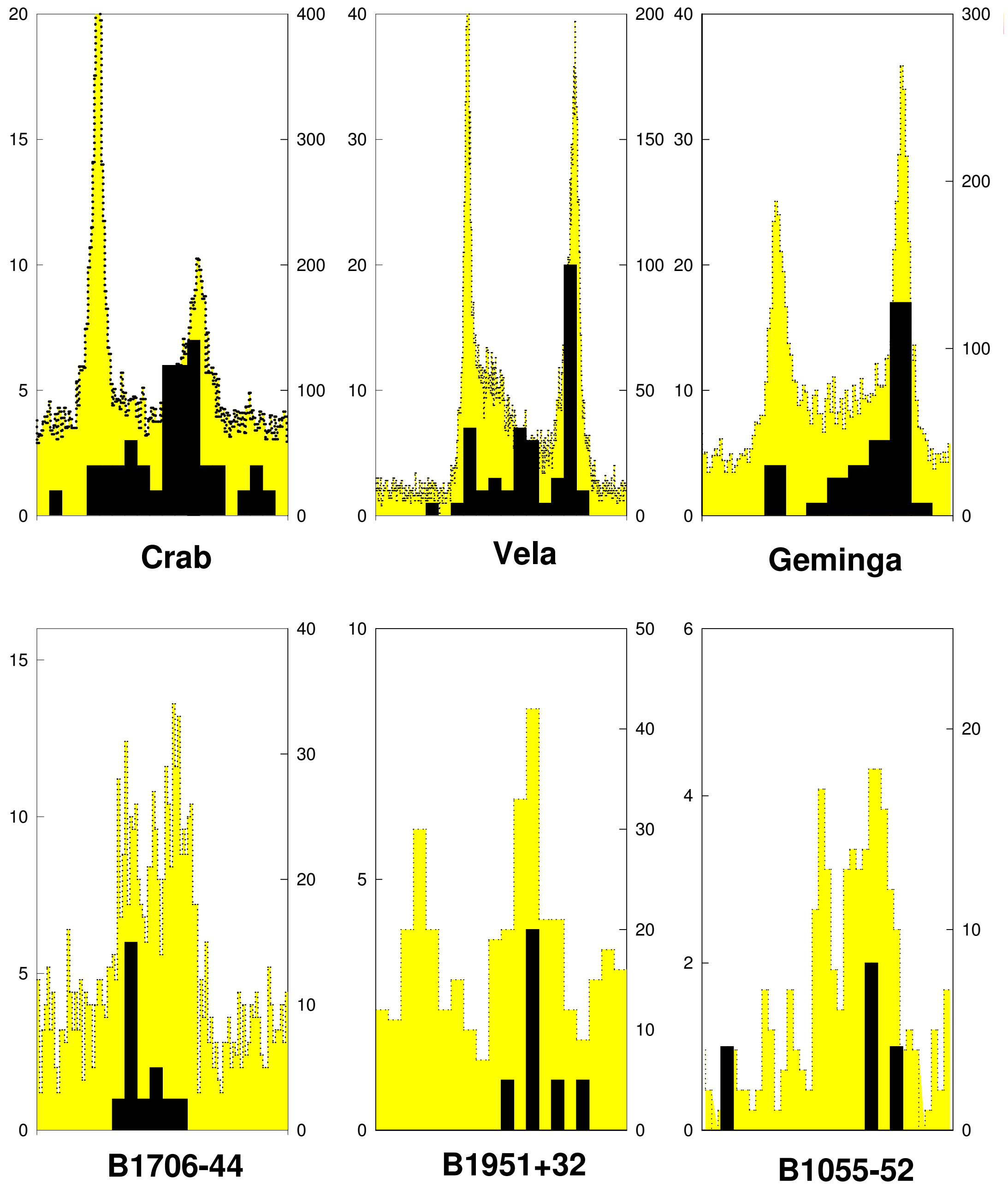

§3 *High-energy emission from pulsars*

However, their inner-slot-gap model (outward extension of the IG model) predicts a negative $E_{||}$ when $\mathbf{\Omega}\cdot\boldsymbol{\mu} > 0$

$E_{||}<0$ induces an opposite gap current from the global current flow patterns.

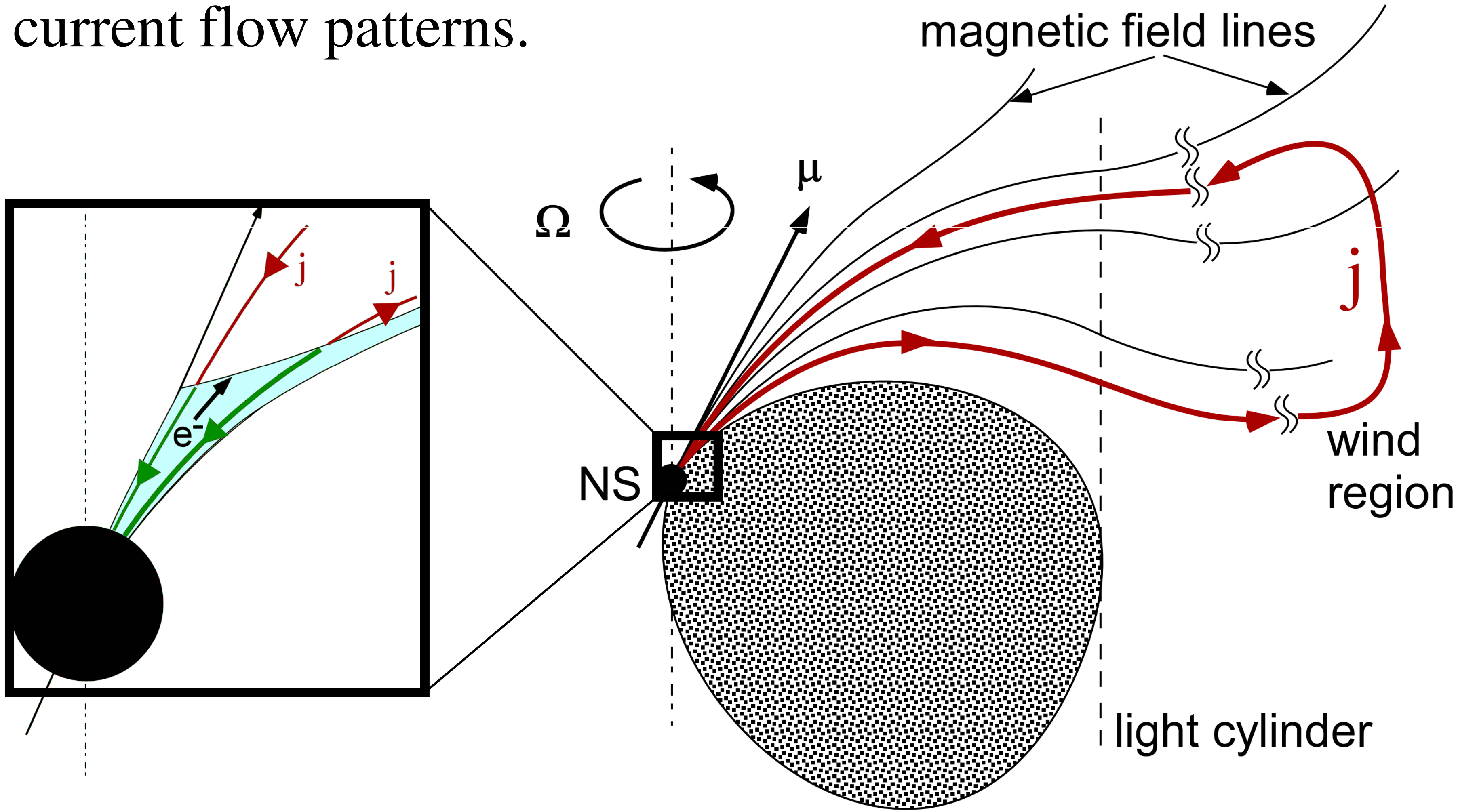

§3 High-energy emission from pulsars

Inner gap: near the magnetic axis

Outer-slot gap: near the last-open field line

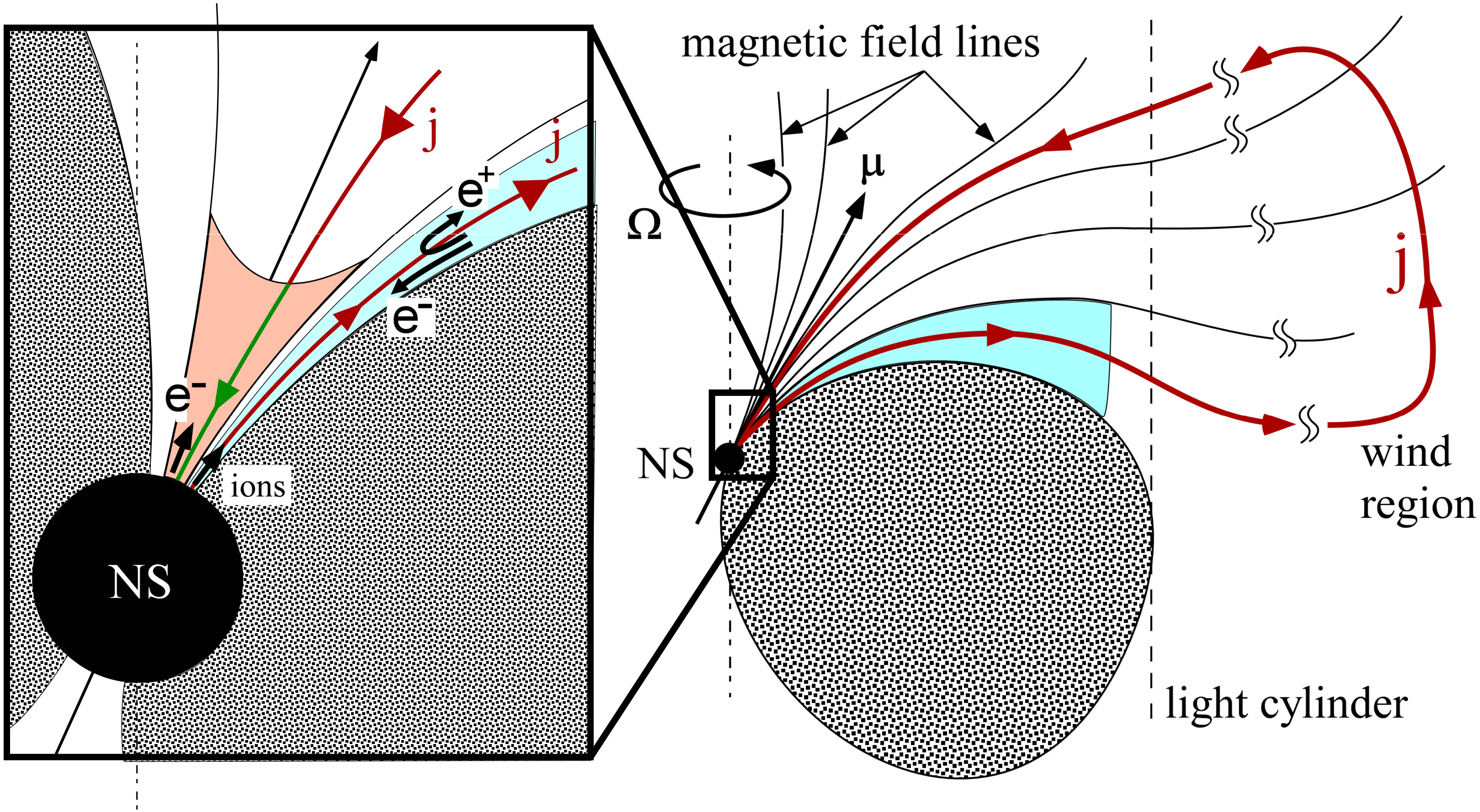

§3 New gap model: Boundary conditions

To solve the set of Maxwell & Boltzmann equations, we must impose appropriate BCs.

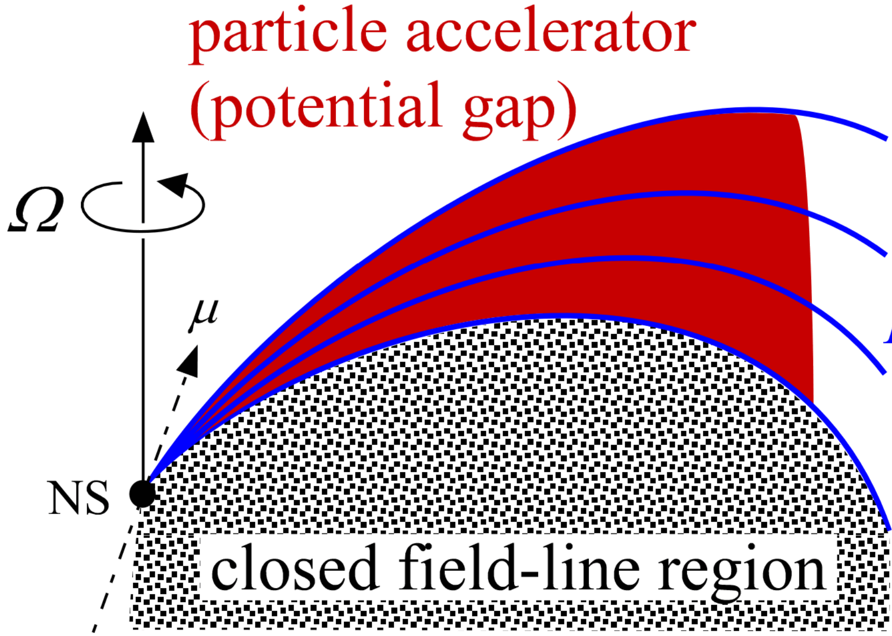

Assume that…

inner boundary
= stellar surface

lower boundary
= last-open field line

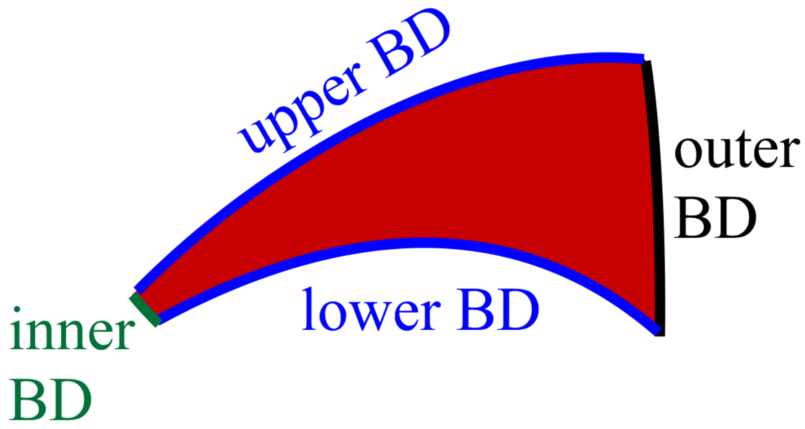

§3 New gap model: Boundary conditions

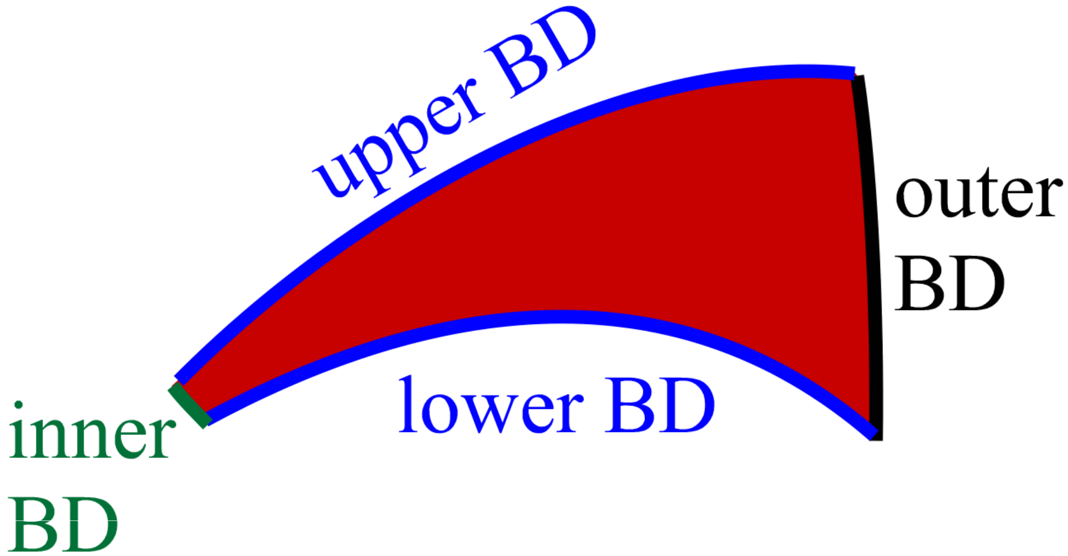

To solve the Poisson eq. for electrostatic potential Ψ,
we impose

$$\Psi = 0 \qquad \text{at inner, lower, upper BDs}$$

$$\frac{\partial \Psi}{\partial x} = 0 \quad \text{at outer BD}$$

§3 New gap model: Boundary conditions

To solve particle/γ-ray Boltzmann eqs., we assume that $e^-/e^+/\gamma$-rays are not injected across the **inner boundary**

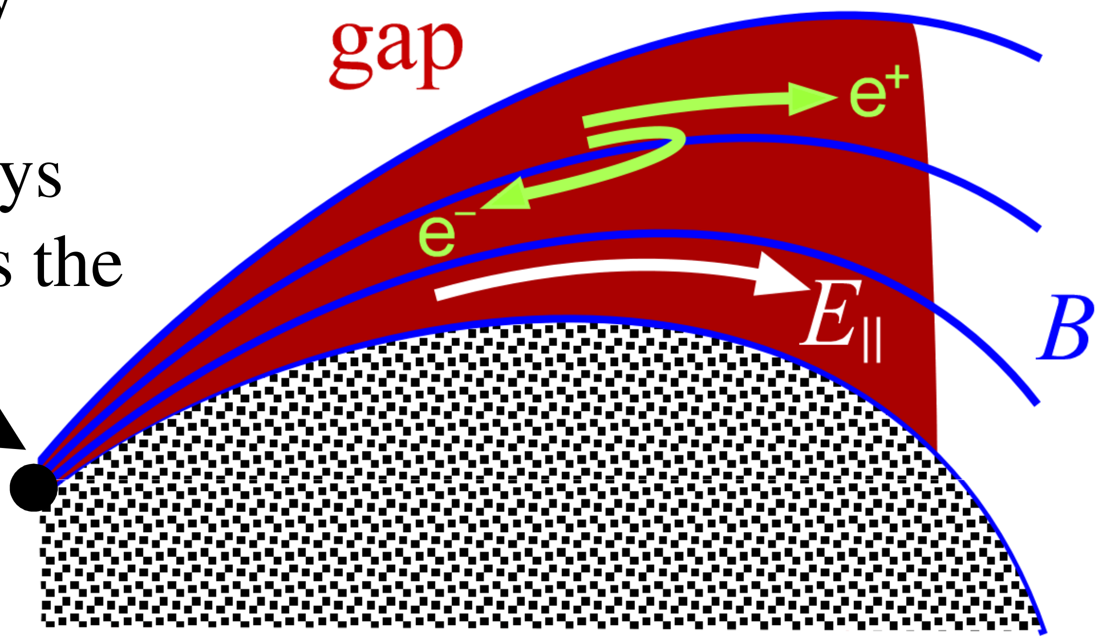

$$N_+(x^{\rm in}, z, \Gamma) = 0$$

$$G(x^{\rm in}, z, E_\gamma, \theta_\gamma) = 0, \quad \text{where } 0 < \theta_\gamma < \pi/2 \text{ (outgoing)}$$

§3 New gap model: Boundary conditions

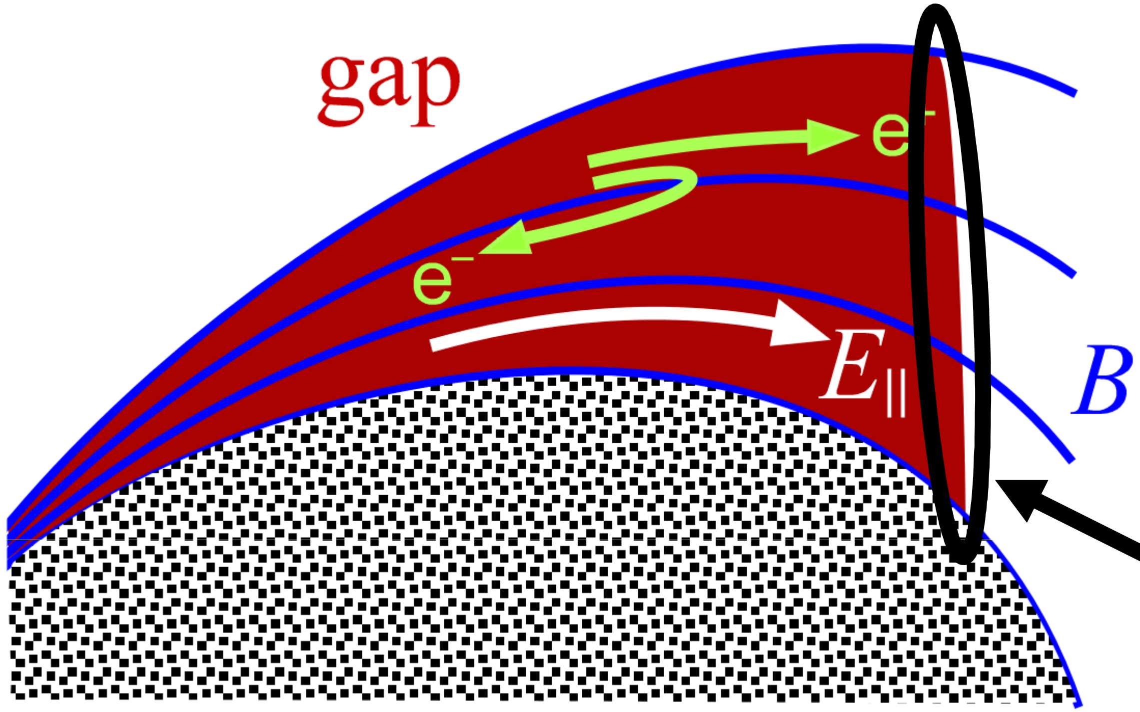

At the **outer boundary**, we also assume no injection of partilces/γ-rays.

$$N\_(x^{\mathrm{out}}, z, \Gamma) = 0$$

$$G(x^{\mathrm{out}}, z, E_\gamma, \theta_\gamma) = 0, \quad \text{where } \pi/2 < \theta_\gamma < \pi \text{ (in-going)}$$

That is, no particle/γ-ray injection across the BD.